Cell Tissue Res (2014) 355:485–514
DOI 10.1007/s00441-014-1810-3

REVIEW

Experimental tools to monitor the dynamics of endothelial barrier function: a survey of in vitro approaches

Joachim Wegener · Jochen Seebach

Received: 12 November 2013 / Accepted: 13 January 2014 / Published online: 2 March 2014

Abstract Endothelial cells line the inner surface of all blood vessels and constitute a selective barrier between blood and tissue. Permeation of solutes across the endothelial cell monolayer occurs either paracellularly through specialized endothelial cell-cell junctions or transcellularly via special transport mechanisms including transcytosis, via the formation of transcellular channels, or by cell membrane transport proteins. Several in vitro assays have been developed in the past few decades to analyze the molecular mechanisms of transendothelial permeability. Measurement of the electrical resistance of the cell monolayer has proven to be particularly suitable for analyzing paracellular barrier function with high-time resolution over long time periods. We review the various permeability assays and focus on the electrical impedance analysis of endothelial cell monolayers. We also address current progress in the development of techniques used to investigate endothelial permeability with high-lateral resolution and under mechanical loads.

Keywords Endothelium · Permeability · Impedance analysis · Transendothelial electrical resistance · Electric cell-substrate impedance sensing

Structure of the endothelial barrier

The endothelium constitutes a semipermeable barrier between blood and tissue. Exchange of molecules between the apical (luminal) and basolateral (abluminal) compartment can occur along trans- or paracellular pathways. The cellular structures that are involved in defining transendothelial permeability and transport will be briefly introduced in the following paragraph as far as they are relevant for the assay discussions below (for more detailed information, see the recent reviews of Aird 2007a, 2007b, 2012; Bates 2010; Hu et al. 2008; Komarova and Malik 2010).

Paracellular transport through the intercellular space is controlled by various types of cell junctions, such as tight junctions (Wallez and Huber 2008) and adherens junctions (Dejana and Orsenigo 2013; Hordijk et al. 1999; Schnittler 1998; Vestweber 2008). The structure and composition of endothelial cell junctions show a large organ-specific variability throughout the human body (Simionescu et al. 1975, 1976). This organ-specific differentiation results in large differences in endothelial barrier function (Aird 2012). External stimuli or the local environment can further modulate the tightness of endothelial cell junctions (Aird 2007a).

Transcellular mechanisms of solute transport include vesicular transport, the formation of transcellular channels or *fenestrae* and transport mediated by specific membrane proteins (Esser et al. 1998; Komarova and Malik 2010; Miller and Cannon 2013; Salmon et al. 2009; Verkman 2006). A major part of the endothelial cytosol is usually occupied by vesicles that are involved in macromolecular transport, e.g., transcytosis of albumin (Aird 2012; Komarova and Malik 2010; Predescu et al. 2007). These vesicles are capable of fusing to establish a vesiculo-vacuolar organelle (VVO; Dvorak and Feng 2001; Vandoorne et al. 2010). VVOs are large enough to connect to the apical and the basal membrane at the same time thereby forming transcellular channels. In a similar way, *fenestrae* form transcellular pores that are covered by a diaphragm. These structures can be found regularly in endothelial cells providing high rates of fluid transport, e.g., in the glomerulus of the kidney or in glandular tissues (Salmon et al. 2009). In addition

J. Wegener
Institute of Analytical Chemistry, Chemo- and Biosensors, University of Regensburg, 93053 Regensburg, Germany

J. Seebach (✉)
Institute of Anatomy and Vascular Biology, Westfälische Wilhelms-Universität Münster, Vesaliusweg 2-4, 48149 Münster, Germany
e-mail: seebach@uni-muenster.de

to these structures, endothelial cells express a wide variety of channels, carriers and transport proteins, such as aquaporins (Verkman 2006) or ABC-transporters (Mahringer et al. 2011; Miller and Cannon 2013), which are also involved in the transcellular transport of small solutes and water.

At least for macromolecules, the endothelial surface layer (Jacob and Chappell 2013; Salmon et al. 2009) and the basement membrane (Salmon et al. 2009) represent additional permeability barriers. Indeed, the endothelial surface layer, which consists in the endothelial glycocalyx and associated plasma components such as albumin, has recently been proposed to represent the major diffusion barrier for large plasma molecules (Becker et al. 2010; Jacob and Chappell 2013).

Whereas the endothelial barrier is usually closely regulated under physiological conditions, a disruption of endothelial integrity under pathological conditions can contribute to edema formation (Aman et al. 2012; Patterson and Lum 2001) and the development of atherosclerotic lesions (Sun et al. 2011, 2012). A deeper understanding of endothelial barrier function and of its physiological and pathological regulation has therefore attracted considerable interest from applied and fundamental biomedical research. This has led to the development of several experimental approaches to quantify endothelial barrier function in vitro; these approaches will be summarized and discussed below.

Quantification of barrier function: methods, models and parameters

The three most closely studied parameters quantifying endothelial barrier function are: (1) the permeability to (macro-)molecular probes providing the permeability coefficient P_E; (2) the permeability to water expressed as the hydraulic conductivity L_P, and (3) the permeability to small inorganic ions described by the transendothelial electrical resistance (TER). These three parameters will be discussed and compared below, together with their individual experimental requirements and current developments.

Permeability coefficient of molecular tracers

A straightforward and well-established approach to probe the efficiency of endothelial barrier function and, thus, the tightness of the intercellular junctions is a simple permeation/diffusion assay (Gunzel et al. 2010; Lohmann et al. 2002). In this set-up, the cells are grown on highly porous filter membranes that support the cell layer mechanically without acting as a significant diffusion barrier themselves. The cell-covered membrane is then placed between two fluid compartments such that any flux of solutes from one compartment to the other is required to pass through the interfacial cell layer. In a typical experiment, a tracer compound is added to one compartment (donor), whereas samples are taken from the other (acceptor) after well-defined time intervals. From the concentration increase of the tracer in the acceptor compartment, one can calculate the permeability coefficient P_E, which represents the barrier properties of the cell layer under study. The permeability coefficient P_E is defined as follows:

$$J = P_E \cdot \Delta c = P_E \cdot \left(c_{Donor} - c_{Acceptor}\right) \quad (1)$$

with the area solute flux J across the endothelium and the (initial) concentration gradient Δc between both compartments. When the area flux J is expressed as [mol/(cm^2·s)] and the concentration is given in [mol/cm^3], the unit of the permeability coefficient P_E is [cm/s]. Strictly speaking, P_E represents the permeability of the cell-covered filter and needs to be corrected for the permeability of the cell-free filter membrane (P_F), which is often negligible but depends on the type of filter. If such a correction is required, the experimentally measured permeability coefficient P_{EXP} is corrected by the permeability of the filter P_F according to Eq. (2) to provide the true P_E value of the endothelial cell layer:

$$1/P_E = 1/P_{EXP} - 1/P_F \quad (2)$$

If filter membranes with low pore densities are used, another factor that has not been considered so far might contribute to the experimentally observed permeability values. Endothelial cells adhering to the filter surface create a thin fluid-filled channel between the cells and filter surface. This channel is usually only 50–200 nm in width. However, it creates an extra diffusion barrier, along the extracellular diffusion pathway across the cell layer and the filter membrane, for the marker compound before it reaches the pores and gains access to the acceptor compartment. This inherent contribution to the overall permeability cannot be corrected by experimental controls. The permeability of the cell-free filters is obviously not appropriate as the channel-forming cell bodies are missing. To the best of our knowledge, nobody has yet reported this extra contribution to expertimentally observed P_E values but the same phenomenon has been addressed and discussed for measurements of the TER, as will be discussed in detail below (Lo et al. 1999).

As long as the probe cannot migrate across the cell membranes and is not actively transported, solute permeation is solely dependent on extracellular diffusion and the permeability coefficient P_E is entirely determined by the functional properties of the endothelial cell junctions and the width of the intercellular cleft. The permeability coefficient P_E is, however, not a general parameter but is specific for a given probe and its molecular properties (Bates 2010; Cohen et al. 1999). Typical probes that are used in such P_E assays are, for instance, dextrans of different molecular weights, sucrose or inulin. These tracers are highly water-soluble, non-membrane permeable and are not actively transported by the cells. Thus, they serve as inert

markers for the accessibility of the extracellular transendothelial diffusion pathways that are limited by the barrier-forming cell-cell junctions. The probes can either carry a radiolabel or fluorescent label for quantification; otherwise, their concentration has to be determined by chromatography.

By using probes of various molecular weights, several authors have tried to investigate the size of pores that are assumed to decorate the junctions making them size-selective (Cohen et al. 1999; Neuhaus et al. 2006). For instance, Zink et al. (1993) studied the transendothelial permeation of markers with various molecular weights and diameters across layers of bovine aortic endothelial cells (BAEC). The authors observed a size-dependence of the permeability coefficient that is only meaningful when two different types of pores exist with approximate diameters of 1 or 17.5 nm. By comparing the measured permeability coefficient P_E of sucrose across BAEC monolayers with the permeability of the same molecule in straight water P_{H2O} ($P_{H2O}=D_{H2O}/dx$; with D_{H2O} as the diffusion coefficient of sucrose in water and dx being the length of the diffusion pathway along the intercellular cleft), they calculated the total area of the cell monolayer that contributes to permeation to be 0.4 %. Similar to this example, P_E values have been used in several different ways to characterize endothelial barrier.

The permeation/diffusion assay has been successfully applied to quantify the permeability of xenobiotics and drug candidates across endothelial and epithelial barriers. Moreover, it has provided valuable insight into the structure and function of endothelial junctions. Despite all these undisputed merits, this widely established and simple assay is integral by nature and as such, it is easily compromised by defects in the cell layer. Even single cell defects can serve as short-cuts for the marker flux and might lead to a serious underestimation of barrier function. Moreover, such a permeation assay usually requires time for the probe to accumulate in the acceptor compartment (Matter and Balda 2003), such that it is not capable of providing real-time information on the status of the junctions. An experimental set-up for automated and time-resolved measurements of P_E has been developed recently (Young et al. 2010). Notably, the assay is integral not only in terms of cell layer defects but also with respect to the permeation pathway and permeation mechanism. It cannot discriminate between paracellular diffusion along the intercellular cleft and a vesicular transport mechanism, for instance, by transcytosis unless well-selected marker compounds are used.

Hydraulic conductivity

The hydraulic conductivity L_p is a different term for the permeability of an endothelial or epithelial cell layer for water. Water flow across an interfacial cell layer is either initiated by an uneven tonicity on either side of the cell layer characterized by an osmotic pressure $\Delta\pi$ (osmotic conductivity) or by a hydrostatic pressure difference ΔP (hydrostatic conductivity). Accordingly, the flux of water J_W across barrier forming cell layers can be described by Eq. (3):

$$J_W = L_p(\Delta P - \Delta\pi) \quad (3)$$

The question as to whether water is transported across endothelial and epithelial cell layers on transcellular routes across the membranes, on paracellular routes across the barrier forming cell junctions, or both has been discussed for a long time. The literature on the subject reveals a highly diverse spectrum of answers that are obviously very much dependent on cell type (endothelial cell or epithelial cells), organ and species. This inconsistency is probably based on the individual lipid composition of the plasma membranes, the presence of aquaporins (water channel proteins) in the membranes and on the presence of water conducting claudins in the tight junctions (Gunzel et al. 2010). The presence of water-permeable aquaporins in the plasma membrane might be either constitutive or highly regulated. For endothelial cells, the formation of *fenestrae* has a major impact on the predominant route of water transport. The experimental discrimination between trans- and paracellular water flux is difficult and has not been solved as yet. One way of retrieving estimates for both flux contributions requires the measurement of the water flux across the apical membrane, the basolateral membrane and the barrier-forming cell layer. Once these values are known, the paracellular water flux can be calculated (Carpi-Medina and Whittembury 1988). The observation of water flux across the upper or lower membrane is accessible by the microscopic analysis of cell swelling or shrinking when the cells are exposed to non-isotonic media either from the upper (luminal) or the lower side of the filter-grown cell layers. Water flux across the entire cell layer is determined by adding, to the bathing fluid, a fluid-phase fluorescent tracer that moves together with the solvent. Changes in the luminal or abluminal fluorescence intensity report the direction and the rate of water transport across the cell layer. The hydraulic conductivity plays important roles in several physiological and pathological processes, such as in glomerular filtration (Deen et al. 2001) or edema formation (Simard et al. 2007).

Transendothelial electrical resistance

General considerations

Another popular way of probing the functional properties of endothelial junctions is based on measuring the electrical resistance of the cell layer when it is placed on a porous filter membrane between two fluid compartments, as described above. Each compartment is equipped with a pair of Ag/AgCl electrodes that are used for injecting a direct current

(DC; I) and reading the associated voltage drop (U) across the cell layer, respectively. The application of Ohm's Law, i.e., R=U/I, provides a resistance value that is then referred to as the transepithelial or transendothelial electrical resistance (TER; Fig. 1). The TER represents the integral resistance of the entire cell layer as a measure of its ionic permeability provided that (1) the resistance of the empty filter insert has been determined independently and is subtracted and (2) that the measured resistance value (in Ohm) is multiplied with the area of the filter (in cm^2) providing the area-specific resistance (in $Ohm \cdot cm^2$) that serves as a characteristic descriptor for the barrier properties of the cells under study (Gunzel et al. 2010).

The advantages of the TER approach are its non-invasiveness and its outstanding time resolution of less than a minute. Accordingly, the status of the barrier can be routinely monitored without any need to sacrifice the culture and monitoring is performed close to real time. However, a few drawbacks and pitfalls are worth considering:

(1) The *TER* approach as an integral method is similarly prone to artifacts caused by absent cells in the cell layer as the determination of the molecular permeability coefficient P_E. Small defects and heterogeneities within the cell layer create a short-cut to current flow and seriously affect TER readings. To illustrate the potency of defects affecting TER, a back-of-the-envelope calculation reveals that one missing cell per hundred cells reduces TER readings from 100 $\Omega \cdot cm^2$ to only 50 $\Omega \cdot cm^2$. In this calculation, the specific resistance of a cell-free filter is assumed to be 1 $\Omega \cdot cm^2$. Unfortunately, filter membranes are usually not optically transparent and the evaluation of the confluence of the cell layer is therefore difficult, sometimes making an interpretation of TER problematic.

(2) A further requirement for the correct determination of TER is a homogeneous electrical field throughout the measurement (Fig. 1a). Unfortunately, even commercially available set-ups do not always meet this requirement. For instance, with the highly popular chop-stick electrodes that are introduced at the periphery of the cell-covered filter, current flows only through an unknown fraction of the entire cell layer, whereas the associated resistance readings are still multiplied by the nominal surface area of the cell-covered filter (Fig. 1b). Under these conditions, TER readings indicate cell layers to be tighter than they really are (Gunzel et al. 2010; Jovov et al. 1991). This potential overestimation of TER attributable to inappropriate electrode geometry and position becomes increasingly more influential the larger the filter membranes are in terms of surface area.

Even if these practical problems are solved, the interpretation of TER readings is not always simple. Many researchers assume that TER readings exclusively reflect the status of the junctions and, thus, the paracellular pathway. However, this assumption is not always valid as transcellular currents (Gunzel et al. 2010; Gunzel et al. 2012; Powell 1981), changes in the cell substrate distance (Lo et al. 1999), or in cell morphology (Claude 1978) can also significantly alter TER. These effects will be discussed below in detail.

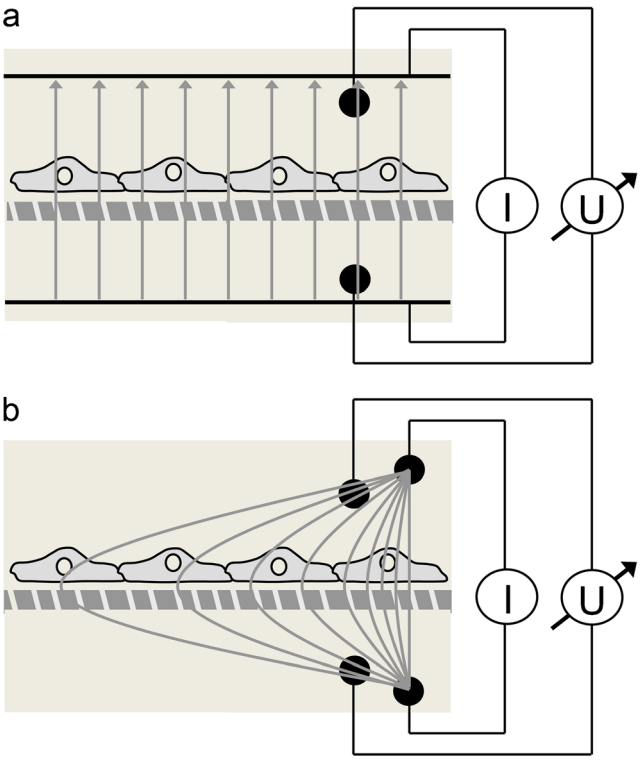

Fig. 1 Electrode set-up to determine transendothelial electrical resistance (TER). Two electrodes are used to apply a direct current (DC; *I*), whereas two additional electrodes measure the associated voltage drop (*U*). TER can then be calculated according to Ohm's law: TER=U/I. **a**, **b** Point-like current electrodes are responsible for inhomgeneous electric fields that can lead to an overestimation of TER

In spite of these limitations, which are important to recognize, TER measurements have been and will be an indispensable tool for learning more about endothelial biology and for studying the functional expression of barrier-forming cell-cell contacts and their regulation. In particular, modern modifications of the basic technique will become important for investigating barrier properties in situ from various perspectives, with a focus on spatial resolution, sample throughput, or information content that goes significantly beyond the integral aspects described above. In the following paragraphs, we will therefore focus on those modern developments and summarize their individual benefits and limitations. Most state-of-the-art approaches no longer rely on DC measurements, because of the constant concern about membrane polarization and net charge displacement. Moreover, DC-based TER measurements require corrections for the resistance of the filter itself and of the medium or buffer solution in which the cells

are bathed. Instead of DC techniques, impedance analysis or impedance spectroscopy has gained increasing impact in cell biology, as this approach uses alternating voltages and currents, which are significantly less invasive but carry more information. The following paragraph will provide a short introduction to impedance analysis boiled down to its most important concepts and parameters. Those readers that are familiar with the technology will find some concepts of impedance analysis highly simplified and some descriptions might not be complete. However, our aim is to summarize and highlight the most critical issues that are relevant for applications in cell biology.

Impedance analysis at a glance

Impedance spectroscopy (IS), also referred to as electrochemical impedance spectroscopy (EIS), is an experimental technique to probe and characterize the electrical properties of bulk materials, composite samples, or interfacial layers non-invasively (Barsoukov and Macdonald 2005; Lvovich 2012; Orazem and Tribollet 2008). This review is entirely dedicated to the application of impedance spectroscopy for studying endothelial barrier function in vitro. A broad survey of the application of EIS to other biological samples such as three-dimensional tissues and organs is given elsewhere (Grimnes and Martinsen 2000).

Fundamental concepts in impedance analysis In a typical IS experiment, a sinusoidal voltage $U(t)$ with angular frequency $\omega = 2\,\pi\,f$ is applied to the system and the resulting steady-state current $I(t)$ induced by this voltage is recorded. The relationship between the applied alternating voltage and the resulting alternating current (AC) can be described by the amplitude ratio of the voltage and current (U_0/I_0) and the phase shift between them (φ). The former is also called the magnitude of the impedance $|Z|=U_0/I_0$ (Fig. 2). Mathematically, the phase shift and magnitude of the impedance can be combined as the complex electrical impedance Z, i.e.,

$$Z = |Z| \cdot e^{i \cdot \varphi} \tag{4}$$

where i is the imaginary unit, which is defined as $i^2=-1$. This complex notation is helpful for deriving and calculating the impedance of electrical networks. However, in the discussion below, we will mostly focus on |Z|.

For an ohmic resistor, |Z| is equal to the resistance R and no phase shift occurs between current and voltage independent of the applied frequency. In contrast, the impedance of a capacitor is frequency-dependent with $|Z|=1/\omega C$ and a phase shift of −90 °C. Accordingly, |Z| for a capacitor is small at high frequencies but increases at lower frequencies. Herein, C denotes the capacitance, which is proportional to the amount of charge that can be stored on the capacitor.

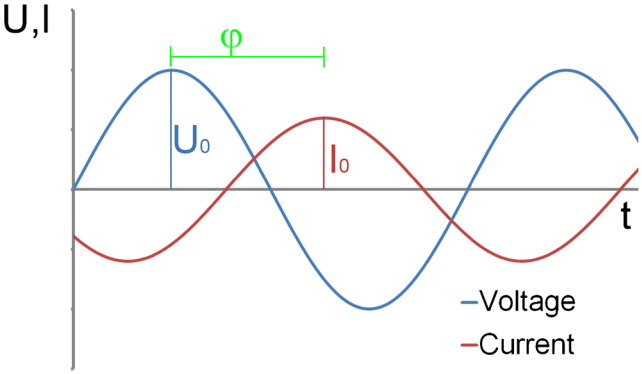

Fig. 2 Relationship between an alternating voltage and an alternating current. In impedance analysis, a sinusoidal current with amplitude I_0 is passed through the system under test. The associated sinusoidal voltage with amplitude U_0 is measured. The electrical properties of the system are then described by the impedance magnitude $|Z|=U_0/I_0$ and the phase shift φ between I and U (t time)

An impedance spectrum provides the impedance of the system under study as a function of AC frequencies and is most commonly presented in the form of a so-called Bode Diagram, which plots the impedance magnitude |Z| and the phase shift φ between current and voltage as a function of frequency on a logarithmic or semi-logarithmic scale. This manuscript will only use the |Z|-panel of Bode diagrams for data presentation. The interested reader is referred to other resources for a more comprehensive survey of additional ways to present spectroscopic impedance data and of their individual advantages (Barsoukov and Macdonald 2005; Freiesleben-de Blasio and Wegener 2006; Lvovich 2012; Orazem and Tribollet 2008; Powell 1981).

Figure 3 shows the impedance spectra of a resistor (R), a capacitor (C), or two different combinations of both. The impedance spectrum of pure resistors is a horizontal line (Fig. 3a) and the spectrum of capacitors is a line of slope (−1) in a log-log presentation (Fig. 3b). The exact positions of both lines depend on the values of R and C. The serial combination of R and C is basically the superposition of the individual spectra (Fig. 3c). More complex networks of R and C produce characteristic spectra that can be derived from the spectra of the individual elements (Fig. 3d). From these examples, it becomes obvious that different electrical circuits show individual impedance spectra. A detailed analysis of the curves by fitting the corresponding transfer functions to the recorded data provides quantitative information about the parameters of the electrical components as will be discussed in the next paragraph.

Data representation and analysis As an example, Fig. 4a shows a typical impedance spectrum recorded for a confluent monolayer of endothelial cells (from Wegener et al. 1999) together with the spectrum of the same but cell-free system in a Bode presentation. The presence of the cell layer increases the impedance in the frequency range between 10^3 and 10^5 Hz

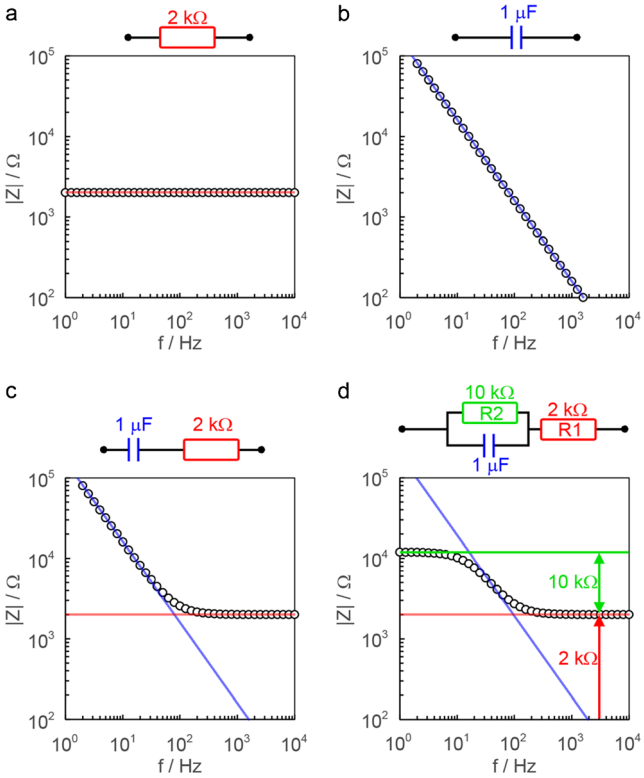

Fig. 3 Impedance spectra of simple electronic networks. **a** $|Z|_R$ of an ohmic resistor is frequency independent: $|Z|_R = R$. **b** $|Z|_C$ of a capacitor is inversely proportional to the frequency of the applied current: $|Z|_C = 1/(2\pi fC)$. Note that this relationship yields a *straight line* with *slope* (-1) in a log-log plot of |Z|(f). **c** In the case of a serial connection, the overall impedance |Z| is approximately the sum of the impedances of the resistor and the capacitor. The *blue* and *red lines* indicate the impedance spectra of the pure elements R and C. Although the impedance of the capacitor is small at high frequencies and can therefore be neglected, it dominates the impedance at lower frequencies. **d** The impedance of this circuit is dominated by the first resistance (*R1*) at high frequencies, because of the low impedance contribution of the capacitor. In the central frequency range, the impedance of the capacitor increases until it exceeds the impedance of the second resistor (*R2*), which dominates the spectra at low frequencies. Note that a quantitative estimate of the parameters of the electrical components of the impedance of R1+R2 is possible. The *blue line* represents the impedance of the pure capacitor

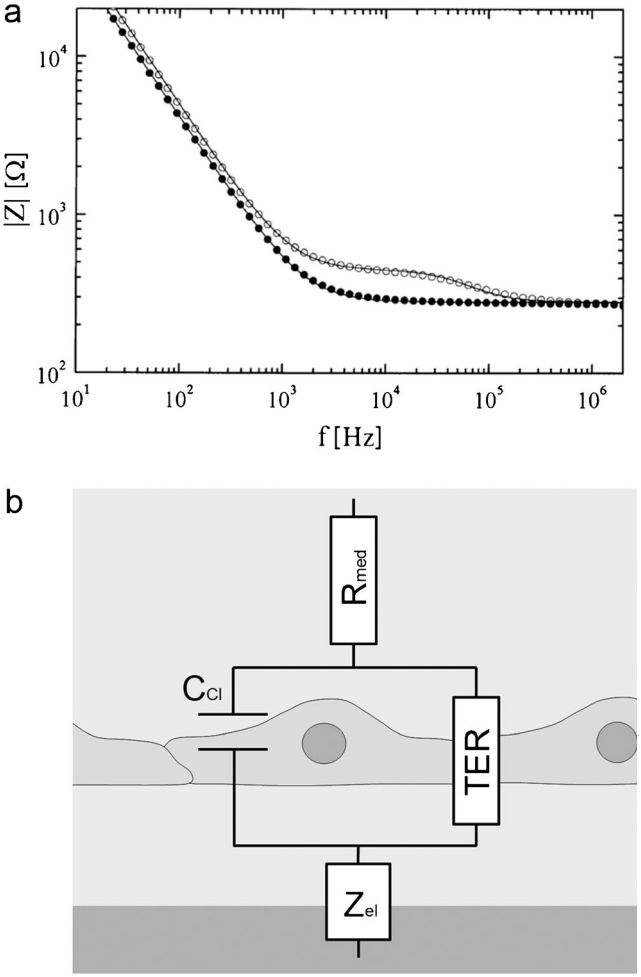

Fig. 4 Impedance spectrum of an endothelial cell monolayer. **a** Impedance spectrum recorded for a confluent monolayer of endothelial cells (*open circles*) together with the spectrum of the same but cell-free system (*filled circles*) in Bode presentation (from Wegener et al. 1999). **b** Equivalent circuit for describing and analyzing the impedance spectrum shown in **a**. The cell layer is represented by C_{Cl} and *TER* (R_{med} resistance of the medium, Z_{el} impedance of the electrode)

relative to the cell-free system. To extract information about the cells under study with more detail than a simple comparison of impedance values, the spectroscopic raw data need to be processed in order to derive parameters that are directly linked to components of the cell layer such as the TER. The most common way to analyze experimental impedance spectra (Fig. 4a) is by means of equivalent circuit modeling (Gunzel et al. 2012; Wegener et al. 2004). An equivalent circuit is an electrical network made up of serial or parallel connections of impedance elements (resistors, capacitors), as known from electronic circuitry, plus additional impedance elements that have been empirically derived for electrochemical systems (e.g., Warburg impedance or Constant Phase Elements). The latter have no correspondence in electronic systems as they represent phenomena such as adsorption or diffusion, which are not relevant for electrons. The equivalent circuit is supposed to represent the electric structure of the sample and to produce the same impedance spectrum (Kottra and Fromter 1984b). With experience, a qualified guess can be made for a proper model based on the characteristic features (e.g., complexity, local slopes, inflection points) in the spectrum. Alternatively, the model is developed from the known electric structure of the sample. For a given equivalent circuit, the frequency-dependent impedance (transfer function) is then derived from the impedance of the individual components and their interconnection by using Ohm's law and Kirchoff's laws.

A suitable equivalent circuit for analyzing the impedance spectrum in Fig. 4a for an endothelial cell monolayer consists in an ohmic resistor to account for the resistance of the culture medium, a parallel combination of an ohmic resistor and a capacitor to describe the electric behavior of the cell layer, and an additional impedance element to describe the electrical

properties of the electrodes used to record the impedance data (Fig. 4a). Ordinary least square algorithms are than applied to adapt the parameters of the equivalent circuit, i.e., the unknown values of the resistors and capacitors within the equivalent circuit, to obtain an optimal congruency between theoretically calculated and the experimentally derived impedance data. If the impedance and phase spectra of the chosen model fit the data well, the parameter values are used to describe the electrical properties of the system and its changes throughout an experiment (Kottra and Fromter 1984b). The equivalent circuit shown in Fig. 4b with its individual impedance elements will be discussed in detail below.

We should mention here that equivalent circuit modeling should be applied with caution. (1) Different equivalent circuit models (deviating with respect to their components or network structure) might produce an equally good fit to the experimental data, although they ascribe the sample a markely different physical structure. In such a case, independent experiments (microscopy, other spectroscopic approaches) are required to obtain further insight into the sample structure and to identify the most appropriate model. (2) One might be tempted to increase the number of elements in an equivalent circuit to achieve better agreement between experiment and model. However, such a model might then become redundant and over-parametrized so that the individual components can no longer be quantified independently. An overly complex model can easily provide artificially good fits to the impedance data with, concomitantly, highly inaccurate values for the individual parameters. Therefore, common sense dictates the use of the equivalent circuit with the minimum number of elements that still describes all details of the impedance spectrum. This is considered to be the non-redundant equivalent circuit model (Kottra and Fromter 1984b).

Another approach to analyze impedance data (though less often applied) is based on the derivation of the impedance of the system by means of differential equations and corresponding boundary conditions. Solution of the differential equation provides the impedance transfer function with the respective model parameters similar to the description by equivalent circuits. The fitting of the transfer function to the recorded data then allows the extraction of the best estimates for the model parameters. Both approaches are essentially only different formalisms to extract better interpretable parameters from the experimental impedance data. The modeling by equivalent circuits is fast and intuitive, whereas the approach based on differential equations is more flexible and adjustable for descriptions of highly complex electric structures.

In most cell-culture experiments, time-resolved information is required. Thus, the spectroscopic information shown in Fig. 5a for a given time should be available for each time point of the experiment. One way of presenting this wealth of information is demonstrated in Fig. 5b. The magnitude of the impedance (z-axis) is plotted as a function of frequency (x-axis) and experimental time (y-axis) in a three-dimensional waterfall plot. Collection of the full spectroscopic information requires time and limits the time resolution to approximately 1 min if only one sample is followed. Several means are available to make data acquisition faster, for instance, by reducing the spectral width or reducing the number of frequencies that are studied along the frequency band, to mention just two. The gain in time resolution is, however, always associated with a corresponding loss of information. In certain cases, it might be sufficient to follow the cells at a single frequency that is properly selected to probe either the capacitive or the conductive pathway through the cell layer. Figure 5c shows the time course of the impedance at a fixed AC frequency. If the AC frequency is properly selected, the impedance reports changes in the current pathway of interest. The spectrum and the time course data are in principle sections from the three-dimensional data stack at a given time (Fig. 5a) or frequency (Fig. 5c).

Impedance analysis of endothelial cell layers on permeable surfaces

Impedance analysis as described above has been applied to endothelial cell layers for decades to quantify the TER and other electric parameters of these cell layers (Erben et al. 1995; Fischbarg and Lim 1973; Lim and Fischbarg 1981; Wegener et al. 1996, 2004). Originally, cells were grown on permeable supports with electrodes reaching into the fluid compartments above (luminal) and beneath (abluminal) the cell-covered filter or grid. Thus, the endothelial cell layer serves as a diffusion barrier and interface between the two fluid compartments, as it does in vivo. In more recent approaches, the cells are grown directly on the surface of the measuring electrodes (Kataoka et al. 2002; Moy et al. 2000; Wegener et al. 1996, 1999). These approaches have certain advantages with respect to sensitivity and some practical issues and will be described separately below.

Historically, four electrodes have been used routinely to determine TER for endothelial cells grown on permeable supports. Two electrodes are used to inject a defined transendothelial current, whereas the two remaining electrodes are needed to record the associated voltage drop across the cell layer (cf. Fig. 1). The voltage-sensing electrodes are commonly placed adjacent to the cell surfaces so that the recorded impedance is dominated by the impedance of the cell layer and does not contain significant contributions from the medium (Gunzel et al. 2010). Notably, in this context, the position of the voltage-sensing electrodes determines those parts of the sample that contribute to the overall impedance of the system. Therefore, the location of these electrodes close to the cell layer avoids significant contributions from the bathing medium. This becomes particularly important as medium resistance can significantly disturb TER readings when highly leaky endothelial cell layers are studied.

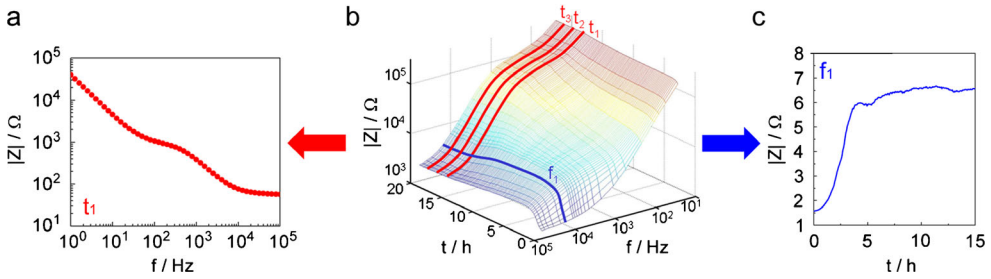

Fig. 5 Various possibilities for representing impedance data as a function of time. The wealth of information provided by repeated acquisition of frequency-dependent impedance data (**b**) along the time course of a cell-based assay can be projected to the frequency (**a**) or time domain (**c**) depending on the focus of the analysis

In two-electrode arrangements, current injection and voltage sensing are provided by just one electrode in each compartment. Such an electrode arrangement has several practical advantages and is justified as long as no (Faradaic) current flows across the electrode interface. As a direct consequence of using only two electrodes, the interface impedance of the electrodes is visible in the impedance spectrum and needs to be included in any equivalent circuit model.

Figure 6 compares the (calculated) impedance spectra of an endothelial cell layer studied with a four-electrode set-up (Fig. 6a) and a two-electrode set-up (Fig. 6b). The inserts indicate the non-redundant equivalent circuit for either system. As discussed above, the cell layer itself is modeled by a parallel combination of the capacitor C_{cl} and the resistor TER. The resistance of the medium R_{med} is arranged in series to this. When four electrodes are employed for data acquisition, the spectrum is fully described by these three parameters. When only two electrodes are used for the measurement, the interface impedance of the electrodes needs to be included. Thus, the equivalent circuit in Fig. 6b has an additional impedance element to account for this electrode impedance. The electrode impedance is most accurately described by a constant phase element (Pajkossy 1994), which represents a non-ideal capacitor and is one of those empirical impedance elements mentioned above that have no relevance for electronic systems. The constant phase element was originally introduced to describe the impedance of noble metal electrodes immersed in electrolyte solutions. The interface behaves similarly but not identically, to an ideal capacitor. Therefore, modeling by a simple capacitor will fail. In contrast, the deviations from ideal behavior are accurately represented by the constant phase element. Non-ideal capacitor behavior is thought to be associated with surface roughness of the electrodes and specific ion adsorption to interfaces (Pajkossy 1994).

Notably, for both electrode arrangements, R_{med} can be distinguished from TER in a single impedance spectrum. Thus, when endothelial cell layers are studied by impedance analysis, instead of DC techniques, blank measurements of the empty filter insert are not needed, as R_{med} is independently quantified from the impedance spectrum of the cell-covered support. Moreover, the resistance of the medium R_{med} can be conveniently used as an independent temperature control, as it changes by approximately 1 % per °C. An inherent temperature control is useful in cases when endothelial cells are challenged by the addition of drugs or xenobiotics. Any unspecific effect attributable to a lack of thermal equilibration is therefore conveniently indicated in the spectrum (Wegener et al. 2004).

The non-redundant model of the endothelium is simply a parallel combination of TER and C_{cl}. TER represents the integral resistance of the cell layer, whereas C_{cl} describes its integral capacitance. The integral capacitance of the cell layer C_{cl} includes the capacitance of the luminal plasma membrane $C_{m,luminal}$ and the capacitance of the abluminal plasma membrane $C_{m,abluminal}$, which are arranged in series along the transcellular current pathway:

$$1/C_{cl} = 1/C_{m,luminal} + 1/C_{m,abluminal} \quad (5)$$

Readings of the cell layer capacitance C_{cl} are amazingly similar for confluent endothelial cells derived from different organs or species and give values of approximately 0.5–0.7 μF/cm^2 (Lim and Fischbarg 1981; Wegener et al. 1996, 1999, 2004). The explanation is based on the experimental finding that the capacitance of unfolded plasma membranes C_m is always close to 1 μF/cm^2 for all cell types. With $C_{m,luminal}$=$C_{m,abluminal}$=1 μF/cm^2, Eq. (5) gives an integral cell layer capacitance of 0.5 μF/cm^2, in close agreement with the experimentally observed values. Thus, the plasma membranes of endothelial cells are entirely unfolded without microvilli or membrane protrusions; otherwise, the cell layer capacitance C_{cl} would be significantly larger than 0.5 μF/cm^2, as has been experimentally observed. These results are supported by electron micrographs in the literature that confirm the absence of microvilli and membrane protrusions on endothelial cells. Higher values for the specific membrane capacitance C_m are commonly observed for transporting epithelia that are known to have invaginated membranes, thereby making transepithelial transport of solutes more efficient. Thus, this impedance-based analysis of endothelial membrane morphology is supported by ultrastructural studies.

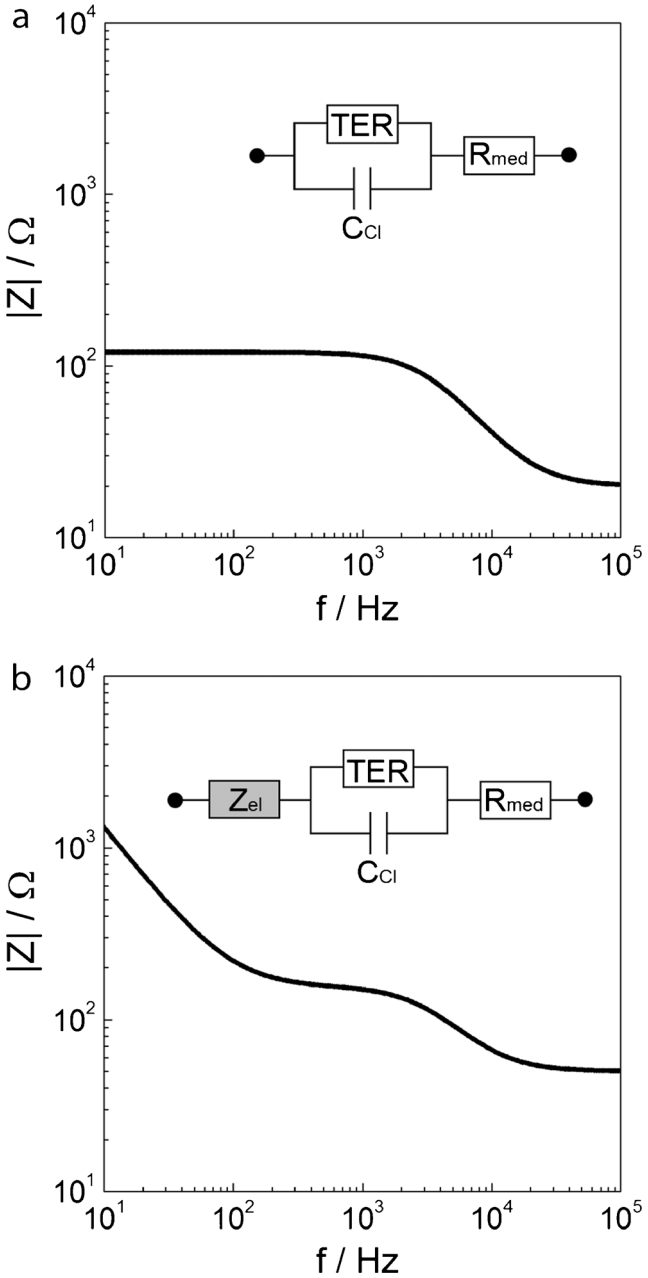

Fig. 6 Various electrode arrangements. Simulated impedance spectrum of an endothelial cell layer measured with (**a**) a four-electrode or (**b**) a two-electrode arrangement. The two-electrode arrangement requires the inclusion of the electrode impedance (Z_{el}) in the equivalent circuit. The serial medium resistance (R_{med}) is commonly higher in two- than in four-electrode arrangements. The cell layer is represented by C_{Cl} and *TER*

TER values mirror the integral resistance of the entire cell layer. However, TER represents approximately the resistance of the paracellular current pathway R_p only for moderately tight endothelia and can thus be used to study the functional properties of barrier-forming cell junctions without any further correction. For extremely tight or extremely leaky endothelial cell layers, TER values are affected by other resistive contributions that are inherently included in TER readings, in addition to R_p. These two limiting cases will be discussed below.

(1) We have briefly introduced above that, in some cases, transcellular currents also have to be considered for a correct interpretation of the TER. This is the case for extremely tight endothelia (e.g., from the blood brain barrier) in which the paracellular resistance R_p has the same order of magnitude as the transcellular resistance R_t. The latter is given by the resistances of the two membranes R_m in series. Thus, in tight endothelia, the current will distribute over the two current pathways: across the junctions or through the membranes dependent on the difference between R_p and R_t. Thus, in more detailed (but redundant) equivalent circuits, TER needs to be replaced by a parallel combination of R_p and R_t. According to Eq. (6), the overall TER will be smaller than either of its two components R_t and R_p.

$$1/\mathrm{TER} = 1/\mathrm{R_t} + 1/\mathrm{R_p} \tag{6}$$

The two contributions inherently included in TER cannot be determined separately by impedance spectroscopy alone. In other words, when TER is the only experimental parameter along the time course of an experiment, changes in TER cannot be unequivocally assigned to R_p or R_t and whether the observed changes in overall barrier function originate from the cell-cell junctions or the membranes remains an open question. Additional information is required to allow for a discrimination of the two parallel resistances. In the 1980s, researchers introduced microelectrodes into the cytoplasm of individual cells within a confluent monolayer or tissue and recorded intracellular voltage profiles as a response to transepithelial current flow (Kottra and Fromter 1984a). Knowledge of the intracellular potential in addition to the luminal and abluminal potentials provided the necessary information to determine trans- and paracellular resistances. Most of this work was carried out on the gallbladder epithelium of *Necturus maculosus* (Kottra and Fromter 1984a). Even though seemingly more difficult in practice, this concept can also be applied to endothelial cells.

Lately, a new approach has been described that combines transcellular impedance measurements with flux analysis of extracellular probes to discriminate between R_p and R_t. Thus far, the paracellular diffusion of membrane-impermeable probes has only been used as an independent experimental indicator of whether the observed changes in TER are indeed caused by changes in the paracellular pathway (Wegener et al. 2000a). If the permeability coefficient P_E decreases while TER increases during an experimental trial (or vice versa), then the

experimental evidence is compelling that the paracellular pathway is affected. No change in P_E while TER increases or decreases indicates that changes in TER are presumably caused by alterations along the transcellular current pathway. Hence, P_E has been used instead as a qualitative parameter to verify or falsify changes in junctional tightness. Krug et al. (2009) demonstrated, in several epithelial cell lines, that the combination of these approaches can be used to quantify R_t and R_p when certain experimental conditions are met. If (1) a permeation marker is used that has roughly the same paracellular permeability as those inorganic ions that are mostly responsible for transepithelial current flow (e.g., Na^+, Cl^-, HCO_3^-) and if (2) an experimental protocol can be found selectively to change the paracellular diffusion pathway but not the transcellular pathway, then R_t and R_p can be determined from TER readings and concomitant measurements of the transepithelial flux J of the permeation marker while the paracellular pathway is opened or closed. The rationale behind this approach is summarized as follows: TER is composed of R_t and R_p as expressed in Eq. (6). A parallel combination of two resistors is more conveniently expressed by using the inverse of the resistance, the conductance G=1/R. Then Eq. (6) translates into

$$G_{ter} = G_t + G_p \tag{7}$$

If the permeation probe matches the requirements, the paracellular conductivity G_p is proportional to the flux J of the probe such that $G_p = s \cdot J$ with the proportionality factor s. Introducing this proportionality into Eq. (7) results in Eq. (8).

$$G_{ter} = G_t + s \cdot J. \tag{8}$$

Equation (8) indicates that measurements of G_{ter} and J during the exclusive opening of the paracellular pathway (e.g., by addition of EGTA to dissociate the calcium-dependent cadherin-mediated cell-cell adhesion) provide a linear $G_{ter}(J)$ relationship with G_t as the intercept on the y-axis and s as the slope of the curve. Under ideal conditions, G_t and G_p can be determined from such an experiment without intracellular electrodes and are expressed as R_t and R_p. As this approach allows the determination of both R_t and R_p, it is referred to as two-path-impedance spectroscopy in the literature. For comparison, the regular transendothelial/transepithelial analysis without any independent experimental data is named one-path-impedance spectroscopy. Even though this assay can be applied to all epithelial and endothelia, the essential experimental requirements of each new tested cell line need to be checked.

(2) At the other end of the TER regime, we find highly leaky endothelial cell types that are hardly capable of establishing a significant diffusion barrier and that are characterized by rather low TER values (Wegener et al. 1999). In this case, another resistive contribution might have an impact on TER readings. When cells adhere and spread out on filter supports, the paracellular current has to flow from the pores underneath the cells and through the narrow cleft between the lower membrane and the filter surface before it reaches the cell periphery with the cell junctions (Fig. 7a).

As the cleft between the membrane and filter surface is only 50–200 nm wide, paracellular current flow will be limited by the length and width of this cleft, in addition to the endothelial junctions (Lo et al. 1999). For equivalent circuits, the overall paracellular resistance R_p has to be broken up into the junctional resistance R_j and the resistance from the cell-substrate adhesion zone R_{adh}, which are arranged in series. Both resistances contribute to R_p but cannot be separately determined by impedance spectroscopy. Obviously, the impact of R_{adh} on TER increases with decreasing porosity (pore density, pore size) of the filter support. Lo et al. (1999) modeled this situation in order to provide an estimate for the importance of this extra resistance, which has been overlooked for a long time. The two models that estimate either the maximum or the minimum value of R_{adh} are based on pore size, pore density, cell radius and the distance between cell membrane and filter surface. In Fig. 7b, R_{adh} is plotted for a typical endothelial cell size and cell-substrate distance as a function of the areal fraction of pores underneath the cells by the two models. Based on these estimates of R_{adh}, we can readily see that this resistance might dominate TER readings for highly leaky endothelial cell layers that have TERs of only a few $\Omega \cdot cm^2$, in particular when filter supports with small pore densities are used. Notably, all assumptions that have been made to derive approximate values for R_{adh} are realistic.

In summary, the impact of R_{adh} increases with the diameter of the cells and the closer that they adhere to the surface of the filter. Moreover, TER readings will be increasingly affected by this phenomenon, the leakier the cell-cell junctions are. The interested reader is referred to the paper by Lo et al. (1999) for further details about the modeling and the limits of applicability. Even though not previously reported, the confined channel between the lower membrane and filter surface will obviously also affect readings of paracellular flux experiments (P_E), as the pathway underneath the cells is as equally constricted for the diffusion of paracellular probes as it is for the movement of inorganic ions. To the best of our knowledge, no experimental strategy has been described so far

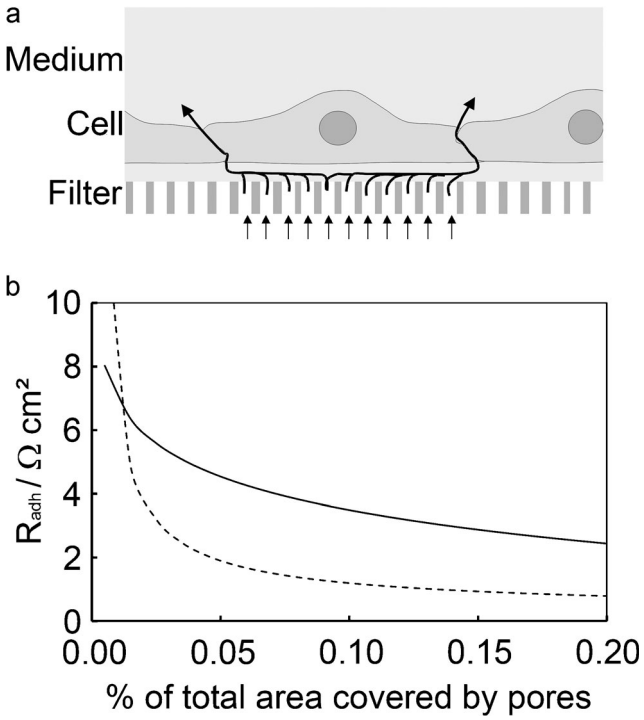

Fig. 7 Resistance of the cell-substrate contact. **a** Representation of the ion current through a cell-covered filter membrane. A small distance between the filter surface and the basal membrane can produce a significant electrical resistance to the current (adapted from Lo et al. 1999). **b** Quantitative calculations based on two different models show that the contribution of this resistance R_{adh} strongly depends on the pore size and density of the filter membrane. A cell radius of 10 μm, a cell substrate distance of 100 nm and a specific medium resistance of 60 Ω×cm were assumed for the calculation

that allows the quantification of R_{adh} experimentally for cells grown on filter supports. When cells are grown on impermeable but conductive surfaces such as gold-film electrodes, the impedance contribution from the cell-substrate adhesion zone can be quantified by impedance spectroscopy, as will be revealed in the subsequent section.

Endothelial cell layers on impermeable surfaces (electrodes)

For a long time, any functional analysis of endothelial barrier function was based on the growing of the cells of interest on permeable substrates acting as an interface between two fluid compartments. This experimental architecture mimics the situation in vivo and allows the study of the permeation or transport of solutes from one side to the other. Moreover, this arrangement has been a necessary prerequisite to place electrodes on each side of the cells in order to apply transendothelial currents, to measure the associated voltage drop and to calculate the transendothelial impedance (compare above). In the 1980s, Giaever and Keese introduced a new technique referred to as electric cell-substrate impedance sensing (ECIS; Giaever and Keese 1984; Giaever and Keese 1991). In ECIS, cells are grown directly on the surface of planar gold-film electrodes, and the dielectric properties of the cells are determined by measuring the impedance of the cell-covered electrodes as a function of frequency, as detailed above for filter-grown cells. Thus, filter membranes are not needed in ECIS as the gold electrodes are concomitantly the growth substrate and electrode. Figure 8 summarizes the basic concept of the ECIS technique.

ECIS uses two electrodes instead of four (cf. above). The two electrodes are deposited on a regular cell-culture dish in a coplanar arrangement and the cells are grown on these surfaces under standard cell-culture conditions. The electrical connection between the two cell-covered electrodes across the dish is provided by the culture medium. The AC current flows between the two coplanar electrodes and passes through the cell layer twice at different locations (Fig. 8). However, the majority of published studies are based on an electrode arrangement with two electrodes that differ with respect to their surface area. By making the counter electrode at least 100× larger than the small working electrode, the impedance of the latter dominates the overall impedance of the entire system with almost no contribution from the much larger counter electrode, as impedance scales with the inverse of the area. Moreover, the small working electrode increases the sensitivity of the measurement (Giaever and Keese 1991). Most data available in the literature have been recorded with circular electrodes of 250 μm in diameter. Measurements with these electrodes are sensitive enough to detect a single cell on the electrode surface.

The use of coplanar gold-film electrodes has several practical advantages:

(1) The electrode-containing dish does not need to be opened for the measurement, as the electrodes are an integral part of the culture-ware. The instrumentation is connected to the electrodes by conductive paths that can be contacted from outside the dish.
(2) The gold-film electrodes used in ECIS are only 50–100 nm thick, so that they are still transparent; the cells on the electrode surface can be studied and documented with conventional light microscopy as is routinely performed with cells in Petri dishes or culture flasks.
(3) The gold electrodes are prepared by thin film technologies and can be easily miniaturized down to the single cell level if necessary. Multi-electrode arrays with individually addressable electrodes within one common cell-culture compartment providing multiple independent measuring sites within a given cell monolayer have been described (Rothermel et al. 2006). These types of electrode arrays provide insight into the distribution of electrical parameters, instead of averaging them over a large cell population. Alternatively, single electrode pairs,

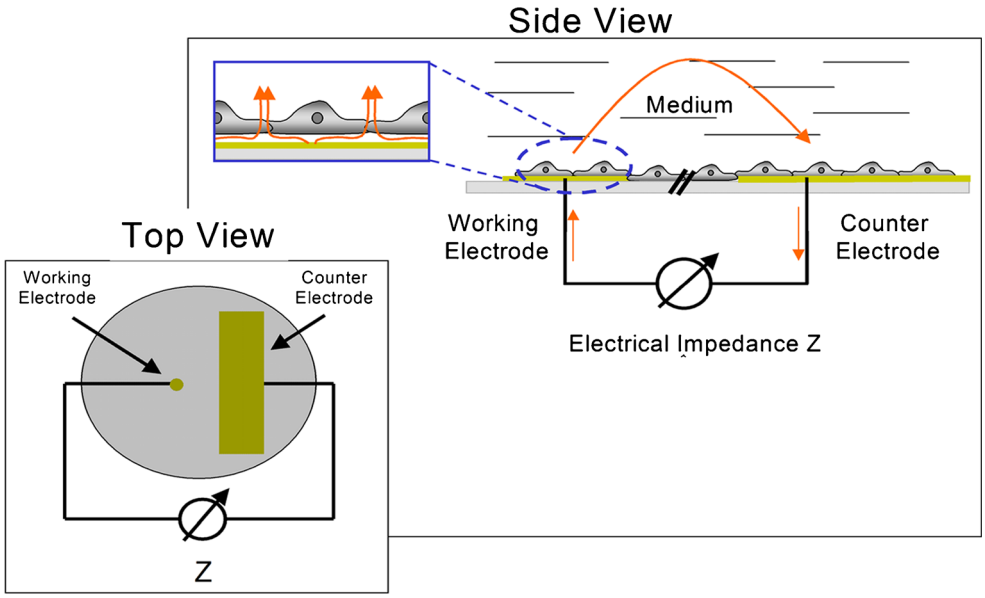

Fig. 8 Representation of the electrode arrangement as used in electric cell-substrate impedance sensing (ECIS) experiments. Because of its larger surface area, the impedance contribution of the counter electrode is extremely small and can be neglected. The measured value of the total impedance is dominated by the cell-covered working electrode

such as the one shown in Fig. 8, have been integrated into each well of 384-well devices, so that ECIS can be used as a readout technology in high-throughput screening campaigns investigating endothelial barrier function (http://www.moleculardevices.com/Products/Instruments/Label-Free-Analysis.html).

(4) Another advantage of using gold-film electrodes over permeable filter supports is the compatibility of the former with other electrochemical techniques that rely on gold-film electrodes. We and others have combined ECIS with techniques such as the quartz crystal microbalance (Janshoff et al. 1996; Steinem et al. 1997) or surface plasmon resonance analysis (SPR; Michaelis et al. 2013), electroporation (Stolwijk et al. 2011), or automated wound healing/migration assay (Keese et al. 2004), all of which are based on markedly different physical principles than those of ECIS and that provide independent information about the cells under study.

(5) Gold has proven to be highly cytocompatible because of its chemical inertness and hydrophilicity under physiological conditions. When pure gold surfaces are incubated with cell-culture medium, L-cysteine from the medium will immediately adsorb to the gold via its thiol group forming a monomolecular layer. As cysteine is a zwitter ion at physiological pH, the surface is then decorated with charged groups providing the observed wettability and hydrophilicity. Proteins adsorbing to cysteine-decorated gold surfaces probably do not denature and keep their native structure and bioactivity. This conclusion is supported by the observed rates of cell spreading upon gold electrodes pre-coated with proteins from the extracellular matrix (ECM; Wegener et al. 2000b). In general, self-assembly processes between thiol-containing molecules and planar gold surfaces can be used to establish various electrode-surface coatings that are extremely stable and robust because of the covalent linkage.

(6) A fair comparison of filter supports and gold-film electrodes must include the information that gold-film electrodes are obviously an impermeable substrate and that cells are only exposed to nutrients, oxygen and differentiation factors from the luminal side. The situation on the electrode surface is, thus, less “in-vivo-like”. The nature of the growth surface might influence endothelial differentiation, even though, to the best of our knowledge, no systematic study has yet been performed to elucidate this possible problem. On the other hand, most routine cultures of endothelial cells rely on Petri dishes and cell-culture flasks, in particular when large cell numbers are used for experiments such as Western Blot analysis. More structural studies of cell junctions by immunocytochemistry are also most often performed with cells grown on coverslips. As all the aforementioned growth substrates are impermeable, it might be more appropriate to use ECIS for functional barrier analysis when structure-function relationships of the cell junctions are to be studied.

Information content and data analysis of frequency-dependent ECIS data In addition to the practical issues discussed above, the question arises as to whether ECIS experiments provide any advantage with respect to the information content of the measurement compared with impedance analysis of cell-covered filter inserts. Indeed, ECIS raw data can be analyzed with the same equivalent circuit (Fig. 4), as has been derived and explained for endothelial cells on permeable filter inserts (Wegener et al. 1999). Thus, TER and C_{cl} can be extracted from ECIS readings. Corrections for blank experiments are not

needed, as the impedance of the electrodes and the bulk electrolyte are included in the spectrum and can be determined separately. Closer inspection of the spectrum revealed that impedance spectra of cells grown on gold-film electrodes contain additional information beyond TER and C_{cl}: the impedance contributions arising from cell-substrate adhesion Z_{adh} can be quantified as an independent parameter from ECIS recordings (Giaever and Keese 1991) and hence, the remaining resistance of the paracellular pathway is the resistance of the cell-cell junctions. Thus, in contrast to impedance measurements from filter-grown cell layers, the impedance attributable to cell-substrate adhesion can be distinguished from the junctional resistance and both can be quantified independently. The reason for this important difference lies in the electrical nature of the growth surface. Whereas filters behave electrically as resistive substrates but not as capacitors, gold-film electrodes behave more like capacitors but not like resistors. As a consequence, the impedance contribution from cell-substrate adhesion is frequency-dependent for gold electrodes but frequency-independent for filters. With the junctional resistance being frequency-independent, like a true pure resistor, it is not distinguishable from the cell-substrate impedance on filters (also frequency-independent) but it is distinguishable from the cell-substrate impedance on gold-film electrodes (frequency-dependent). Figure 9 summarizes calculated impedance spectra that show the change of the spectrum when the cell-related parameters are changed systematically.

In each figure, one parameter is changed, whereas all others are kept constant. The cell-related parameters in ECIS are the resistance between cells R_b (assuming that $R_p << R_t$), the membrane capacitance C_m, and the impedance arising from cell-substrate adhesion, which is characterized by a parameter α with

$$\alpha = r_c \cdot (\rho/d)^{0.5}. \quad (9)$$

In Eq. (9), r_c denotes the radius of the cells, ρ is the specific resistivity of the medium, and d is the distance between the lower cell membrane and electrode surface. The corresponding model that describes the impedance of cell-covered gold-film electrodes was derived by Giaever and Keese, the inventors of ECIS, in 1991. Modeling the impedance underneath the cells requires that a qualified assumption is made about the morphology of the cells, as the current flow between the lower cell membrane and electrode surface is position-dependent. The extracellular current is assumed to flow radially into the spaces formed between the basal membrane of the cell and the electrode surface before escaping into the bulk solution along the intercellular cleft. As a consequence, the model cannot be expressed correctly in the form of equivalent circuits in principle. Instead, Giaever and Keese (1991) derived a set of differential equations for disk-like cells with a radius r_c hovering at a distance d above the electrode surface. Details concerning the derivation of this model are given elsewhere (Giaever and Keese 1991). Figure 9 establishes that changes in R_b (Fig. 9a) and α (Fig. 9b) induce individual changes in the impedance spectra. Thus, they can be determined independently.

Application of ECIS in endothelial biology ECIS and the ECIS model have been successfully applied to a range of experiments in endothelial biology (Table 1). The summary below primarily highlights different assay types. It is not meant to be a complete survey of all studies involving the use of ECIS as a tool for the analysis of endothelial barrier function.

ECIS has been applied to monitor signal transduction in endothelial cells for many different scientific purposes. It has proven to be particularly useful as a label-free monitoring device for studying G-protein-coupled receptors (GPCRs). The cell layer impedance has been shown to change upon stimulation of GPCRs on the cell surface and the observed impedance change can be used to establish dose–response relationships, to perform inhibitor studies and to pinpoint the signal transduction pathway associated with the stimulated receptor (Wegener et al. 1999). ECIS and similar label-free techniques are currently considered as highly potent and promising research tools for studying the functional selectivity of GPCRs, expressed by endothelial cells or others (Scott and Peters 2010).

By virtue of its location at the interface between the blood and the interstitial fluid, the vascular lining is the entry site for

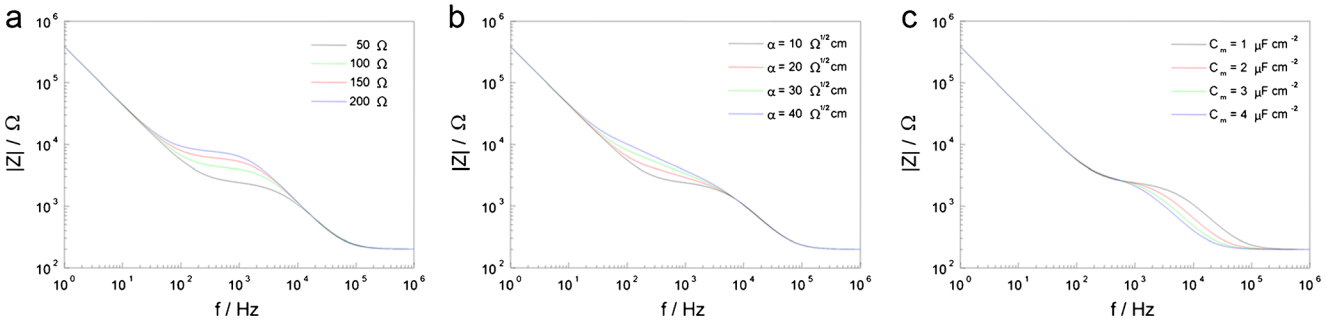

Fig. 9 Parameters of the ECIS model. Simulated impedance spectra demonstrating the individual influence of (**a**) the resistance between cells (R_b), (**b**) the impedance arising from cell-substrate adhesion (α) and (**c**) the membrane capacitance (C_m)

Table 1 Electric cell-substrate impedance sensing (*ECIS*)-based assays in endothelial biology (*GPCR* G-protein-coupled receptors, *EC* endothelial cell, *PKC* protein kinase C, *HUVEC* human umbilical vein endothelial cell, *LPA* lysophosphatidic acid, *SP1* sphingosine-1-phosphate, *ECM* extracellular matrix)

Assay type/application	Extracted information	Endothelial type	Reference
Monitoring GPCR activation and second messenger	Dose–response relationships, antagonistic studies	Bovine aorta EC	Wegener et al. 1999
	Receptor-independent side effects, second messengers involved	Human pulmonary microvessel EC	Tsukahara et al. 2000
	Impact of PKC on barrier function	Pulmonary artery	Fordjour and Harrington 2009
Extravasation of disseminated tumor cells or immune cells	Correlate to metastatic potential	HUVEC	Keese et al. 2002
	Transmigration route	Porcine brain capillary EC	von Wedel-Parlow et al. 2011
Modulation of barrier function	Permeability changes upon exposure to LPA and SP1	Rabbit cornea EC	Yin and Watsky 2005
	Permeability changes by ionizing radiation	Human coronary artery EC	Young and Smilenov 2011
	Barrier modulation by glucocorticoid exposure	Human retinal EC	Keil et al. 2013
Interaction with components of ECM	Impact of endogenous ECM on endothelial differentiation	Porcine brain capillary EC	Hartmann et al. 2007
Monitoring apoptosis	Comparison of ECIS to biochemical apoptosis assays regarding assay sensitivity	Porcine brain capillary EC	Arndt et al. 2004
Barrier analysis during exposure to shear stress	Impact of laminar shear stress	HUVEC	Seebach et al. 2007
	Impact of turbulent flow	Bovine aorta EC	DePaola et al. 2001
Cytotoxicity	Impact of Cytochalasin B on barrier and cell dynamics	HUVEC	Opp et al. 2009
	Impact of industrial chemicals on cell morphology; long-term toxic response	Bovine pulmonary artery EC; bovine lung microvessel EC	Curtis et al. 2009a, 2009b
	Response to oxidative stress	Murine brain EC (bEnd3)	Betzen et al. 2009
Angiogenesis	Wound repair in response to pro-angiogenic compounds	Human vascular EC (HVEC)	C.L. Liu et al. 2013
Monitoring cell-culture conditions	Impact of CO_2 fluctuations in incubator on cell morphology	Bovine pulmonary EC (B3B3)	Lo et al. 1994
Interaction with pathogens	Relative pathogen penetration	Human brain microvessel EC	Grab et al. 2009
	Barrier modulation by pathogens	HUVEC	Taylor et al. 2013

immune cells and disseminated tumor cells into deeper tissues. Many in vitro assays addressing the efficiency of this transmigration process or the molecules involved are based on confluent endothelial cell layers, which are pre-established on permeable supports (Boyden chamber) and which are then challenged with the migrating cell type. Efficiency of transmigration is commonly quantified by counting the number of cells that successfully cross the endothelial cell layer and reach the lower fluid compartment underneath the filter. Several studies have shown that ECIS readings provide a unique perspective on the transmigration process, because of its superior time resolution and information content. Keese et al. (2002) studied the extravasation of tumor cells with various metastatic potentials by ECIS recordings. Prior to the assay, human umbilical vein endothelial cells (HUVECs) were grown to confluence on the employed gold-film electrodes. The confluent monolayer was then challenged with the suspended tumor cells, while endothelial barrier function was monitored by continuous ECIS recording. The data revealed that the impedance of the HUVEC monolayer was only affected when the HUVECs were exposed to tumor cells with established metastatic potential. Non-metastatic tumor cells applied at the same dose only induced insignificant changes of the cell layer impedance. Conditioned media from the same cell lines did not produce a similar result, so that the conclusion was proposed that physical contact between the tumor cells and endothelial cells is required for efficient extravasation. Moreover, time-resolved ECIS recordings and subsequent modeling revealed that metastatic tumor cells were capable of opening the endothelial cell junctions (parameter R_b) several hours before the endothelial cells started to contract and round up from the surface (parameter α). The transmigration of neutrophils across the blood–brain barrier was also studied by ECIS experiments by von Wedel-Parlow et al. (2011). Suspended neutrophils were added to pre-established monolayers of brain capillary endothelial cells (BCEC) that were experimentally stimulated to show an inflammatory phenotype. Inflammation was verified by checking the differential expression of inflammation markers such as platelet endothelial cell adhesion molecule. When neutrophils encountered endothelial cells expressing an inflammatory phenotype, barrier function was not affected, whereas ultrastructural studies showed neutrophils entering the cell body. The authors concluded from the experimental evidence that neutrophil extravasation through the blood–brain barrier occured on transcellular pathways (von Wedel-Parlow et al. 2011).

The strength of the ECIS technique is that it is able to quantify endothelial barrier function non-invasively and with extremely good time resolution that can be reduced to a few seconds. When suspended endothelial cells are seeded onto the electrodes, both cell adhesion to the growth surface and the subsequent expression of barrier-forming cell junctions can be monitored from ECIS readings at various frequencies. Therefore, Hartmann et al. (2007) used ECIS to analyze the impact of glia-derived extracellular matrices on the expression of a blood–brain-barrier phenotype with tight sealing of the intercellular junctions. First, various glia cell types (astrocytes, pericytes) were grown to confluence on the surface of the electrodes. Subsequently, the cell bodies were removed by hypotonic lysis leaving the native ECM of these cells behind. Suspended BCECs were then seeded onto these preconditioned electrodes that had been decorated with the ECM of various glia. An ECM derived from BCEC was used as a control, whereas ECMs obtained from aortic endothelial cells were included to check for a potential negative impact of macrovascular ECM on barrier function. ECIS readings gave the expected results. Although glia-derived ECM was capable of strengthening barrier function over control values, such function was decreased below control values by aortic ECM. These in vitro data confirm that the ECM contains molecular clues that are important for endothelial differentiation (Hartmann et al. 2007).

When cells die either by apoptosis or necrosis, their morphology undergoes highly characteristic changes. Whereas apoptotic cells shrink without rupture of the plasma membrane following a genetically encoded pathway of self-destruction, necrotic cells swell until the osmotic pressure ruptures the cell membrane leading to cell lysis. Both processes clearly affect the tightness of the cell layer and should be mirrored in ECIS recordings. Thus, apoptosis of BCEC was chemically triggered by the addition of cycloheximide (CHX) (Arndt et al. 2004). BCEC responded immediately to the addition of CHX indicating a fast onset of apoptosis. Within less than 8 h, endothelial barrier function had completely disintegrated. When the cells were co-incubated with anti-apoptotic agents such as hydrocortisone, the CHX-induced breakdown of barrier function was slowed down. Modeling of multi-frequency ECIS data revealed that the junctional resistance R_b was reduced shortly after CHX addition; cell rounding and detachment occurred several hours subsequently. In addition to the simple monitoring of apoptosis, one of the specific questions of the study was to compare the time course of barrier breakdown with the time course of caspase activation and DNA fragmentation, with the latter being hallmarks of apoptosis. A comparison of the time course of barrier tightness with the activation of caspase-3 and the levels of DNA fragmentation indicated that barrier function was completely destroyed before caspase-3 activity or DNA-fragmentation had reached their individual maximum. Indeed, barrier function was significantly reduced even before any notable increase caspase-3 activity could be measured. The mechanism of this extremely fast breakdown of barrier function is still under investigation but minute amounts of caspase-3 seem to be sufficient to activate specific intracellular hydrolases that target proteins of the cytoskeleton. Because of the isometric tension in endothelial cells, only small changes in the cytoskeleton might

significantly affect the balance of the "pull-and-push" forces that give the three-dimensional shape of the cells and the mechanical stability of barrier-forming cell junctions.

Barrier function and endothelial morphology

Even in cases when TER predominantly reflects the tightness of interendothelial junctions, we need to bear in mind that simple morphological changes of the cells without any change in the organization and constitution of the junctions can lead to changes in TER. This phenomenon is based on the finding that changes in cell morphology affect the linear amount of paracellular elements per unit area (lp), which is defined as the length of all cell borders between adjacent cells for a given area (Claude 1978). Consideration of a unit area covered with either large cells or with small cells is highly instructive. When the specific resistance per micrometer of junction is identical in both cases, TER readings will be lower for the smaller cells than for the larger ones simply because the smaller cells provide more micrometers of paracellular pathway: the longer the linear amount of junction, the more pathways are available for the current to pass across the cell layer.

Elongated cells show a higher ratio of cell perimeter to surface area compared with circular cells. Accordingly, the linear amount of junction lp is higher than that for a circular cell covering the same surface area. Thus, a morphological switch from circular to elongated increases lp and might lead to an increased paracellular permeability and a corresponding decrease in TER. In vivo endothelial cells show different morphologies within the vascular tree: whereas endothelial cells of the arteries and capillaries are elongated and align in the direction of flow, endothelial cells of the veins display a more circular morphology. In vitro, the morphology of cultivated endothelial cells can be controlled and switched by various stimuli such as shear stress (Seebach et al. 2007), cyclic stretch (Dartsch and Betz 1989; Naruse et al. 1998), supernatants of mononuclear cells (FitzGerald et al. 1987), or various cytokines (Emmanuel et al. 2013; Heffernan et al. 1994; McKenzie and Ridley 2007; Stolpen et al. 1986; Table 2). In this context, two morphological parameters have been used to describe cell elongation quantitatively (Fig. 10). The aspect ratio (AR) is defined as the ratio between the major and the minor axis of the ellipsoid cell. The structure index (SI) is given by:

$$SI = 4\pi A/\left(P^2\right). \quad (10)$$

where A denotes the area of the cell and P is the perimeter. For a perfectly round cell, both parameters are equal to 1. Elongated cells have an AR larger than 1, whereas the SI lies between 0 and 1. Table 2 lists some studies that have investigated the elongation of endothelial cells upon treatment with various stimuli. The quantitative relationship between lp and the morphological parameters AR and SI is shown in Fig. 10b. For example, a change of SI from 0.9 to 0.7 will increase lp by approximately 15 % and reduce the TER accordingly, even if the structure and composition of the junctions remain unchanged. A shear-stress-induced moderate TER decrease has been shown to be attributable to an increase in lp and not to be caused by an opening of the cell-cell junctions (Seebach et al. 2007). Notably, this dependency is not restricted to TER but influences all parameters that describe paracellular barrier function. We therefore highly recommend that changes in paracellular barrier function are correlated with a microscopic analysis of endothelial cell shape.

Comparison and complementarity of the various methods

A comparison of the various assays for characterizing endothelial barrier function would be most informative if all assay types had been applied to the same cell species under exactly the same experimental conditions. These examples are, however, hard to find. To the best of our knowledge, no example exists that compares all of the above-mentioned approaches for a given cell type. Several years ago, our group studied the impact of increasing levels of cAMP on the barrier properties of the choroid plexus epithelium (Wegener et al. 2000a). Changes in barrier function were quantified by measuring the flux of fluorescein isothiocyanate (FITC)-labeled dextrans combined with impedance analysis of the same cells before and after the flux experiment. The study was completed by ECIS recordings of plexus epithelial cells that were grown on gold-film electrodes. Even though this example is taken from the epithelial world, the conclusions of an inter-assay comparison should also apply to endothelial cells.

Figure 11a shows the outcome of the paracellular flux experiment with 4-kDa-FITC-dextran (FD-4) as a probe. FD-4 is only capable of diffusing across the cell layer along paracellular pathways and is therefore well suited to report on changes therein. Choroid plexus epithelial cells were grown to confluence on permeable filter inserts before the FD-4 probe was added to the apical (donor) compartment at time zero. The concentration of FD-4 in the basolateral (acceptor) compartment was determined at regular time intervals and plotted as a function of time (Fig. 11a; filled symbols represent the data for control conditions, whereas open symbols were recorded in the presence of 100 μM CPT-cAMP, a membrane permeable cAMP-analog). Under control conditions, the probe accumulated faster in the acceptor compartment than in the presence of CPT-cAMP indicating a tightening of the paracellular pathway. The same cell layers that were used in this experiment were studied by impedance spectroscopy before and after the permeation assay. The insert in Fig. 11a shows the change in TER in response to the exposure to CPT-cAMP. TER readings obviously doubled from almost 100 $\Omega \cdot cm^2$ to 200 $\Omega \cdot cm^2$.

Table 2 Stimuli that induce cell elongation (*HUVEC* human umbilical vein endothelial cell, *IL* interleukin, *TNF* tumor necrosis factor, *TGF* transforming growth factor, *HAEC* human aortic endothelial cells, *BAEC* bovine aortic endothelial cells, *1* estimated from graph, *2* original as circularity [=1-SI])

Reference	Cell type	Stimulus	Structure index	Aspect ratio	Remark
Heffernan et al. 1994	HUVEC	Control	0.86		1,2
		IL-1α (24 h, 50 U/ml)	0.66		1,2
		IL-1β (24 h, 50 U/ml)	0.65		1,2
		TNFα (24 h, 10 ng/ml)	0.57		1,2
Emmanuel et al. 2013	HUVEC	Control	0.6–0.9		2
		TNFα (24 h, 588 pM)	0.3–0.8		2
		TNFα (24 h, 588 pM) + TGFβ (24 h, 40 pM)	0.2–0.6		2
Dartsch and Betz 1989	Minipig aorta EC	Control		1.8	
		15 % stretch (24 h, 1 Hz)		6.8	
Naruse et al. 1998	HUVEC	Control		1.3	
		20 % stretch (4 h, 1 Hz)		2	
Brower et al. 2010	HAEC	Control		2	1
		shear stress (24 h, 8 dyn/cm^2)		4.08	
Kadohama et al. 2006	BAEC	Control	0.76		
		shear stress (24 h, 14 dyn/cm^2)	0.5		
		shear stress (24 h, 20 dyn/cm^2)	0.47		

The second messenger did not induce any changes of the cell layer capacitance C_{cl} from control values of approximately 2.3 μF/cm^2, indicating no significant change in plasma membrane morphology during CPT-cAMP exposure. According to Eq. (5), the cell layer capacitance C_{cl} corresponds to an average capacitance of the two membranes of 4.6 μF/cm^2, which is almost five times higher than values reported for unfolded membranes (1 μF/cm^2). Consistently, electron micrographs showed a dense population of microvilli on the apical surface that made the true membrane surface approximately five-fold larger than its projection to the growth substrate. Figure 11b provides the results of an ECIS experiment during the exposure of choroid plexus epithelial cells to 100 μM CPT-cAMP. The raw data were analyzed with the ECIS model as described in detail above. Consistent with the analysis of filter grown cell layers, no significant change of the membrane capacitance C_m (not shown) occurred in the presence of CPT-cAMP. The resistance between cells, R_b, representing the paracellular current pathway, increased from 95 Ω·cm^2 to 160 Ω·cm^2 within 120 min. The impedance contribution arising from the cell-substrate adhesion, expressed by the parameter α, increased from 24 Ω$^{0.5}$·cm to 38 Ω$^{0.5}$·cm in just 30 min. Hence, the ECIS data confirmed a tightening of the epithelial barrier (R_b) also a change within the narrow cleft between the lower cell membrane and electrode (α). The change in α might indicate a closer adhesion of the cells to the surface or a change in ionic composition in the adhesion zone.

The comparison of all three assays is instructive and demonstrates that a combination of these assays is often worthwhile and thereby overcomes individual limits and restrictions. The following details of an assay comparison should be considered:

(1) The time-resolved ECIS experiments reveal that barrier function changes by almost 50 % within 30 min. As the permeation assay is integral and requires the accumulation of the permeation marker in the acceptor compartment, it is too slow to detect fast changes in barrier function on this time scale. Moreover, because of the continuous permeation of the marker from the donor to the acceptor compartment and because of the unavoidable loss of the chemical gradient of the marker, long-term changes in barrier function with time are impossible to follow. Impedance analysis, however, provides a label-free snapshot of the status of the barrier with a time resolution that can be pushed to a few seconds.

(2) The chemical properties of the permeation marker allow an undisputed assignment of the transport pathway involved. Whereas TER and ECIS readings cannot rule out changes in the transcellular pathway as an explanation for the observed electrical changes, the permeation experiment is unequivocal in this respect.

(3) Impedance analysis in either mode reveals that increased levels of intracellular cAMP do not affect the cell layer capacitance or, in terms of cell morphology, microvilli and membrane invaginations. This information might not be important in this particular case but can be in others, for instance, when changes in TER are caused by changes in the membrane resistance R_m attributable to

an increase or decrease in membrane area available for current flow.

(4) The observed increase of TER is significantly larger than the increase of the resistance between cells R_b as determined by ECIS readings. If we assume that TER represents solely the paracellular pathway ($R_p << R_t$) for the choroid plexus epithelium, then TER represents the sum of the resistance of tight junctions, the paracellular cleft, plus that arising in the cell-substrate adhesion zone R_{adh}. The individual contributions cannot be separated for filter-grown cell layers. Both contributions are, however, individually quantified for cells grown on gold-film electrodes and the corresponding ECIS analysis demonstrates that the resistance in the cell-substrate adhesion zone is indeed increased under the influence of CPT-cAMP. This is the reason that the increase in TER, which summarizes both contributions, is greater than the increase in R_b. The same explanation holds true for the values of TER and R_b under control conditions. Data interpretation with respect to TER, R_b and α as described above assumes that the cells behave essentially similarly on gold electrodes as on permeable filter inserts.

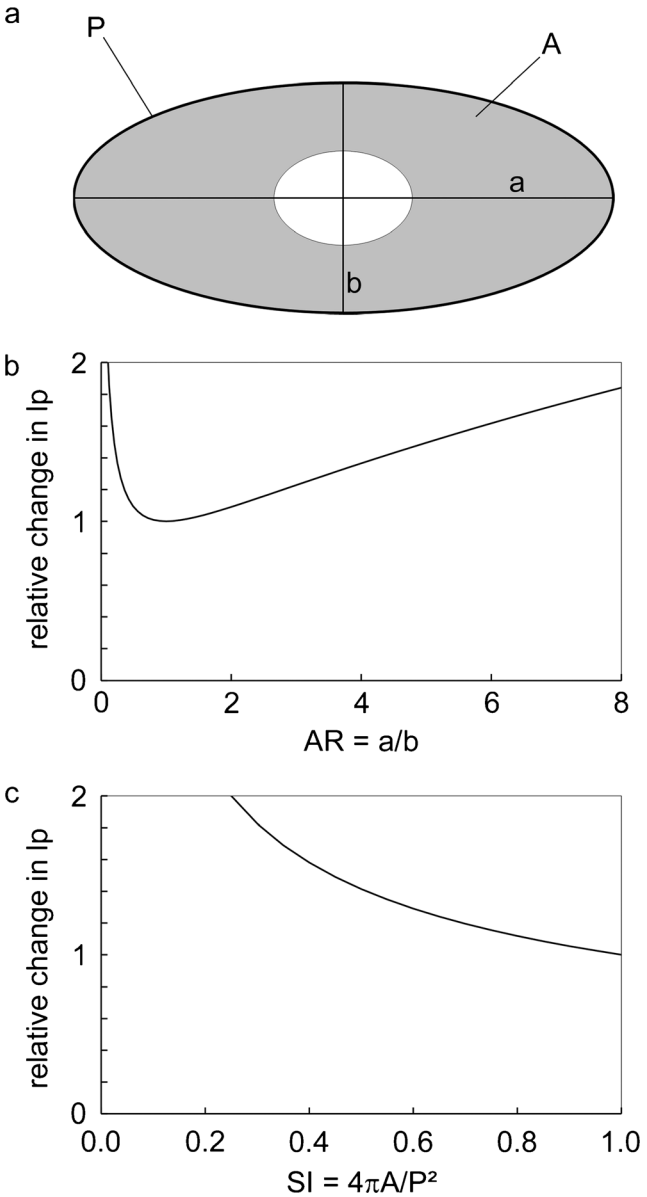

Fig. 10 Correlation between cell elongation and the linear amount of junction per unit area (*lp*). **a** Representation of an elongated cell with cell area (*A*), cell perimeter (*P*), major axis (*a*) and minor axis (*b*). **b** Correlation between the aspect ratio (*AR*) and lp. **c** Correlation between structure index (*SI*) and lp for the assumption of a constant cell area

Imaging permeability with lateral resolution

The methods discussed so far determine the overall permeability of a cell layer and do not account for local heterogeneities in paracellular barrier function (Sill et al. 1992). The available electrochemical and microscopic techniques that allow the study of the heterogeneities within cell monolayers, single cells defects (e.g., attributable to apoptosis), or even heterogeneities within individual cell junctions will be summarized in the following section.

The experimental problem involved in the study of endothelial barrier function with spatial resolution was first addressed by Phelps and DePaola (2000) who studied its dynamic adaptation to various fluid flow profiles along the endothelial surface. In their study, spatially inhomogeneous flow fields, which can be typically found in vivo at arterial bifurcations and at certain distances to it, were used to simulate specialized vascular structures. Experimentally, endothelial cells were grown on permeable supports and exposed to laminar flow. However, a step disturbance was introduced perpendicularly to the direction of fluid flow. Close to this step disturbance, the laminar flow field was disturbed, whereas it recovered laminar characteristics at positions more distant to it. To study the barrier characteristics of endothelial cells at various positions of this inhomogeneous flow field, the cells were exposed to flow for 5 h before the abluminal side of the cell-covered filter membrane was placed on an agarose gel. A permeability marker (FITC-dextran, 70 kDa) was added to the apical compartment and was allowed to diffuse across the cell layer for 30 min. The permeating probe accumulated in the agarose gel at the site of its permeation. Mapping of the macromolecular permeabilty strongly relied on the use of an agarose gel for the acceptor compartment, as it reduced the lateral diffusion of the probe for later analysis without a loss of spatial resolution. After 30 min of assay time, the cell-covered filter was removed from the agarose gel. The latter was then cut into lanes parallel to the step disturbance. The amount of permeation marker in each of these gel lanes was then

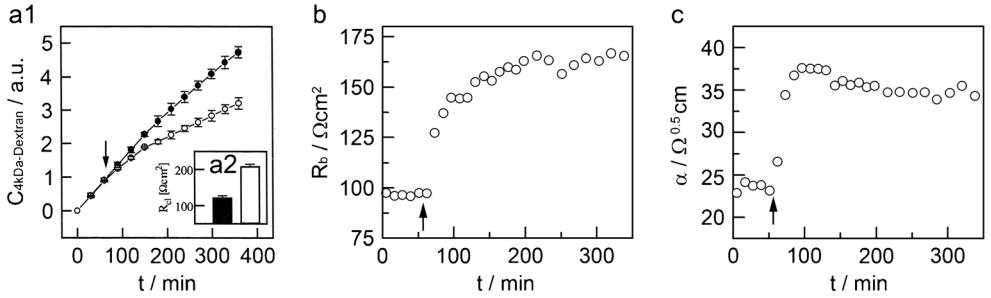

Fig. 11 Correlation between various parameters for paracellular barrier function. **a1** Time course of the concentration (*C*) of a 4-kDa fluorescein isothiocyanate (FITC)-labeled dextran (*a.u.* arbitrary units) in the acceptor compartment of a permeability assay when confluent choroid plexus epithelial cells are exposed to 100 μM CPT-cAMP (membrane permeable cAMP-analog; *open circles*) or control conditions (*filled circles*). *Insert* (**a2**) Comparison of TER values of the same cells at the end of the permeation assay. TER values support the observed decrease in transendothelial permeability. **b** Time course for the resistance between adjacent cells (R_b) as recorded by ECIS readings when confluent choroid plexus epithelial cell layers grown on top of gold-film electrodes were treated with 100 μM CPT-cAMP at the indicated time (*arrow*). **c** Time course for the cell-substrate adhesion parameter α as recorded by ECIS readings when confluent choroid plexus epithelial cell layers grown on top of gold-film electrodes were treated with 100 μM CPT-cAMP at the indicated time (*arrow*)

determined seperately by fluorescence readings and revealed that endothelial barrier function was significantly affected by the disturbed flow fields compared with undisturbed laminar flow (Phelps and DePaola 2000). The lateral resolution of this permeability assay was low and well beyond the size of a single cell. However, it was good enough to document the differences in endothelial barrier function with respect to the position of the cell in a macroscopically heterogeneous fluid flow field; it was also possible to assign a local permeability coefficient P_E to flow conditions at the very same spot. In this study, the authors also used local readings of the TER to support their findings. By placing measuring electrodes with an area of 0.6×10^{-3} cm^2 at various positions relative to the step disturbance, local variations could also be demonstrated in the electrical tightness of the endothelium dependent on the local flow conditions (Phelps and DePaola 2000).

A significant improvement with respect to the lateral resolution of macromolecular permeability maps was achieved by using mesoporous silicon surfaces as a growth substrate for barrier-forming cell layers (Michaelis et al. 2012). The silicon substrates contain a dense and highly ordered array of pores that are much smaller than the diameter of the cells and only open to the side facing the cell layer. The pores are approximately 1 μm in diameter and 10 μm in depth. The lattice constant is approximately 4 μm. These pores serve as an array of femtoliter cuvettes in which the permeating compound can accumulate at the site at which it permeates across the cell layer. Lateral diffusion is made impossible by the walls of the pores (Fig. 12a).

Imaging the filling of the pores with a confocal microscope reveals the local permeability of the cell layer at subcellular lateral resolution. Thus, the approach not only identifies leaks within the cell layer but also provides an experimental discrimination between trans- and paracellular diffusion. If a given marker compound diffuses across the cell layer along paracellular pathways, it only accumulates in those pores that are located underneath the cell borders. Accordingly, the distribution pattern of the probe in micrographs circumscribes the individual cell bodies within the cell monolayer (Fig. 12b). In contrast, a marker compound permeating across the cell layer along transcellular pathways via the membranes provides a laterally homogeneous filling of all pores underneath the cell bodies. Accordingly, the corresponding microscopic images show a homogeneous fluorescence pattern along the entire substrate. When individual cells are missing in the

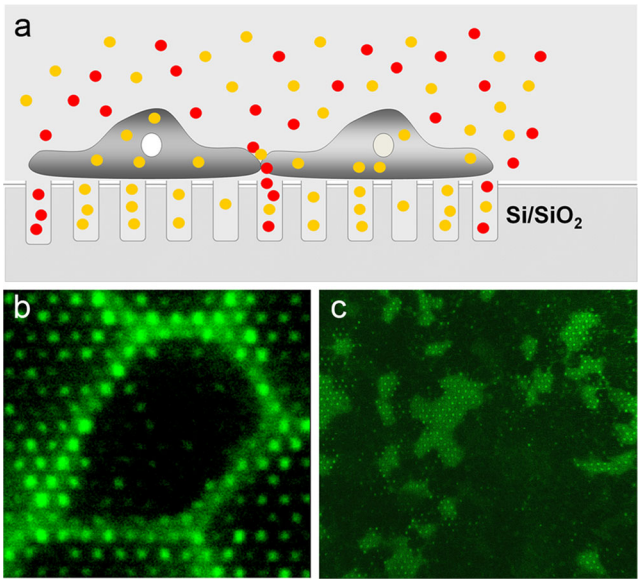

Fig. 12 Mesoporous silicon growth substrates for analysis of the permeability of cell layers with lateral resolution. **a** A barrier-forming cell monolayer is cultivated on a mesoporous silicon chip (*Si/SiO₂*). The permeating probe (*colored circles*) is collected and detected at the site of permeation after accumulation in the pores. **b** Confocal fluorescence micrograph of a mesoporous substrate covered with a confluent Madin-Darby-canine kidney (MDCK) II cell layer after incubation with FITC-dextran in the extracellular buffer. **c** At lower magnification, single cell defects are easily recognized by an increased fluorescence signal. From Michaelis et al. (2013)

monolayer because of cell death or cell replacement, this short-cut in barrier function is easily identified by a corresponding filling of pores underneath the defect area, whereas pores underneath adjacent cells show an expected regular filling pattern for the probe under study (Fig. 12c).

In the so-called XPert assay (Dubrovskyi et al. 2013), the lateral resolution is further refined. This method makes use of molecular recognition between the growth substrate underneath the cells and the permeating probe in order to slow down any lateral diffusion away from the site of permeation. Thereby, the probe becomes immobilized at the site of permeation and the permeation route is conserved for later microscopic inspection. The authors used gelatin that was doped with biotin, before it was deposited on the bottom of a cell-culture plastic. Afterwards, the cells were grown on the surface until a confluent monolayer was established. FITC-labeled avidin served as permeation marker. Wherever FITC-avidin traversed the endothelium from the luminal to the abluminal side, it was immobilized at the site of permeation by binding to the covalently immobilized biotin. The lateral resolution of this approach is only limited by the density of biotin moities underneath the cells. One major advantage of this approach is that the probe is almost irreversibly immobilized to the biotinylated gelatin, so that other analytical approaches might become applicable. A disadvantage of this assay is its limitation to avidin (possibly also streptavidin) as a permeation probe. This inflexibility hinders more systematic studies such as an analysis of the permeation characteristics dependent on the nature, size, or charge of the probe.

A totally different approach used to image local permeabilities of barrier-forming cell layers has been reported recently by Bergner and colleagues (2013). Instead of using luminescent probes and light microscopy to image the permeation pathway across barrier-forming cell layers, these authors exposed the cells to a redox-acitve molecule and imaged its transfer across the cell layer by means of scanning electrochemical microscopy (SECM). In SECM, a small (working) electrode with a diameter in the range of several hundreds of nanometers is scanned across a sample surface, while oxidation/reduction reactions occur at the electrode tip, which is kept at a constant, properly selected electrode potential. The associated redox current is determined by the local concentration of the redox-active species. Thus, this technology is capable of mapping the distribution of the redox-probe with subcellular resolution in situ. A recent review summarizes the advances of the basic technology (Bergner et al. 2013). For mapping the permeability charactersitics of a given cell layer, the cells are grown on permeable filter supports. The abluminal (lower) compartment is then doped with the redox-active marker compound, which is allowed to permeate across the cell layer, while the luminal surface of the cell layer is scanned continuously with the tip of an SECM that carries a properly selected electrode potential. Whenever the permeating redox probe diffuses across the cell layer, its appearance on the luminal side is locally detected in situ by SECM. The redox current determined for a given pixel is proportional to the local concentration of the probe providing a permeability map of the cell layer under study. Bergner et al. (2013) successfully demonstrated the permeation of redox markers along para- and along transcellular routes, respectivey. These two different permation pathways are mirrored in the SECM micrographs.

For this particular application, the SECM technique is still in its infancy but it is capable of providing spatially resolved permeation profiles for the probe under study, with a lateral resolution in the order of several hundred nanometers. However, permeation studies are restricted to probes that are electrochemically active and that can be oxidized or reduced at decent potentials. Moreover, the time that is needed to scan a macroscopic area of the cell layer is still long and determines the time resolution of the measurement to a range of several tens of minutes. Thus, the method is blind to fast changes in endothelial barrier function. A highly promising and most interesting application is the concomitant use of two redox-active marker compounds that permeate across the cell layer exclusively along trans- or paracellular pathways. If the redox potentials of these two markers are sufficiently separated, trans- and paracellular transport can be measured in one scan by sequential application of the individual electrode potentials for each pixel. This and other imaging modes might render SECM an interesting extension of the existing experimental techniques for studying endothelial barrier function.

The mapping of transepithelial resistances with microscopic lateral resolution has been performed by using microelectrodes for local and confined potential measurements at the cell surface, while a uniform and homogeneous clamp current has been established across the entire cell layer (Gitter et al. 1997, 2001). This technique of local resistance measurements at microscopic resolution is referred to as conductance scanning or voltage scanning. By scanning the voltage-sensing electrode across the cell layer, resistance maps can be established and local defects can be identified in the barrier function of the cell layers (Gitter et al. 2001). Moreover, the resistance of the paracellular current pathway across the cell junctions can be distiguished from the resistance of the transcellular current pathway across the membranes and each one of them can be separately quantified (Gitter et al. 1997). In particular, this discrimination between para- and transcellular resistance makes conductance scanning an important tool for studying tight-junction-specific alterations. As discussed above, such discrimination is in principle not possible with the integral TER approach. In addition to (1) the introduction of intracellular micro-electrodes or (2) the application of two-path-impedance analysis (see above), conductance scanning is a third experimental technique for quantifying these two

resistances R_t and R_p separately. The technique has been employed to study defects in epithelial cell layers (Gitter et al. 2001) and to follow the local changes in electrical tightness when apoptosis occurs within a barrier-forming cell sheet (Bojarski et al. 2000; Schulzke et al. 2006).

Several modifications of the basal conductance scanning technique have been described and with scanning ion conductance microscopy (SICM), the lateral resolution has been improved significantly below the micrometer limit. SICM has become a powerful competitor of scanning force microscopy, as it is capable of imaging the topography of cells with several tens of nanometer resolution without contact (Gorelik et al. 2004; Novak et al. 2009). In SICM, this high-resolution topographical imaging is based on the change of the entrance resistance at the pipette tip when it comes close to the sample surface. Thus, the measured conductivity can be used as a feedback signal for piezo-steppers and height resolution. However, this sensitivity for topography makes it harder to identify true changes in local conductivity that are not based on topographic features. Accordingly, one of the major breakthroughs that have paved the way to several new applications is the combination of local conductance measurements with an independent topographic imaging by shear force or scanning force microscopy. The independent topographical information makes local conductance readings much easier to interpret, as the topography at any given pixel is known and the readout is exclusively determined by the local impedance of the system under study (Böcker et al. 2007). Korchev and coworkers combined SICM with patch-clamp principles in order to use this device to measure the conductance of ion channels on single cells (Gorelik et al. 2002).

Endothelial barrier function upon mechanical stimulation

Mechanical forces

TER, permeability coefficients for marker compounds (P_E) and the hydraulic permeability (L_P) have been successfully used to describe the influence of a large variety of stimuli on endothelial barrier function, including pro-inflammatory cytokines, growth factors, interactions with tumor cells and viral or bacterial pathogens, to name but a few. A complete survey of all stimuli and their individual impacts on barrier function would greatly exceed the scope of this review. Most of these studies have been performed under static or mild hydromechnical load conditions that are similar to those typically found in the venous system. However, in vivo, the vessel walls, particular in the arterial system and in the capillaries, are continuously exposed to significant mechanical forces that are generated by the blood stream, such as hydrostatic pressure, stretch and shear stress. This special hemodynamic environment plays an important role for the development and structure of the intima and the media and a distortion of these forces might also contribute to the development of atherosclerosis (Anssari-Benam and Korakianitis 2013). Early in vitro studies were able to demonstrate an impact of such forces on the endothelial cytoskeleton (Franke et al. 1984), endothelial cell junctions (Yoshida et al. 1995) and vesicle formation (Davies et al. 1984), indicating that mechanical forces are able to change paracellular and transcellular permeability. Thus, the impact of biological, chemical, or physical stimuli on endothelial barrier function under flow conditions should be straightforward to study and several experimental set-ups have been developed in the last few decades to investigate endothelial barrier function in the presence of well-defined mechanical forces. The impact of such forces on endothelial differentiation in general and on the expression of a barrier-forming phenotype in particular are summarized below.

Hydrostatic pressure

When endothelial monolayers cultured on a permeable substrate are subjected to enhanced hydrostatic pressure, the hydraulic conductivity will decrease significantly within minutes (Parker et al. 2006; Suttorp et al. 1988, 1989). This so-called sealing effect is accompanied by a reorganization of tight junction molecules (DeMaio et al. 2004). However, the effect has also even been observed for fixed cells (Turner 1992). Thus, the sealing effect is probably attributable to a combination of biological reorganization and the passive mechanical deformation of structures that contribute to endothelial barrier function. In addition to this sealing effect, the water flow through the intercellular cleft driven by the pressure difference can act as an additional stimulus for the endothelial cells (Tarbell et al. 1999). This endothelial cleft shear stress itself induces an increase in hydraulic conductivity, which can be inhibited by blocking the endothelial nitric oxide synthase (NOS; Tarbell et al. 1999).

Since both water and ion conductance are assumed primarily to occur along paracellular pathways, hydraulic conductivity and TER are two frequently used parameters to determine junction-mediated barrier function. However, TER measurements are usually performed without a transmural pressure and in the absence of an endothelial cleft shear stress. Indeed, the sealing effect has been shown not to be accompanied by an increased electrical resistance of the monolayer (Turner 1992). Thus, direct conclusions from effects of TER on hydraulic conductivity are difficult to draw and vice versa.

Shear stress

Fluid shear stress generated by the blood flow has, in particular, been found to play an important role in endothelial physiology. Several cellular structures have been suggested to contribute to endothelial shear stress sensing (Davies 1991;

Poelmann et al. 2008): matrix (Terada 2008), cilia (Hierck et al. 2008; Nauli et al. 2008), cell junctions (Conway et al. 2013; Y. Liu et al. 2013) and glycocalix (Fu and Tarbell 2013; Tarbell and Shi 2013). They all might be involved in transducing mechanical momentum into biochemical signals (Davies 1997; Ishida et al. 1997; Takahashi et al. 1997; Traub and Berk 1998).

Laminar flow profiles have beneficial effects and act as anti-apoptotic (Dimmeler et al. 1996) and anti-inflammatory (Chen et al. 2003) stimuli. They promote endothelial cell differentiation (Riha et al. 2005) and lead to the release of vasodilating agents (de Wit 2010; Lamontagne et al. 1992). Disturbed and turbulent flow profiles, however, are associated with increased cellular turnover (Davies et al. 1986; Xu 2009) and endothelial dysfunction (Chien 2008).

To study the effects of laminar fluid shear stress in cell-culture models, two different in vitro set-ups have been developed. In the parallel plate flow chamber approach, the endothelial cells are cultured on the bottom of a narrow channel and a pump is used to generate a laminar flow over the cells (Grabowski et al. 1985; Koslow et al. 1986; Levesque and Nerem 1985). In the cone and plate rheological system, the endothelial cells are cultivated on a circular plate. A laminar flow is generated by rotating a cone with a small angle relative to the horizontal and this cone is positioned directly above the plate (Buschmann et al. 2005; Dewey et al. 1981; Schnittler et al. 1993; Fig. 13). With this set-up, even complex flow profiles can be applied homogeneously over large cell-culture areas (Buschmann et al. 2005). This opens up the possibility of performing biochemical analyses that require large amounts of cells such as pull-down or immune-precipitation assays (Seebach et al. 2007). In both approaches, an accurate geometry of the shear space is crucial for guaranteeing a laminar flow and for preventing the development of undesired turbulence and disturbed flow profiles.

The major challenge for investigating the barrier function of endothelial cell layers in such systems is to gain access to the basal compartment without disturbing the geometry of the shear space. For TER measurements, this can be achieved easily by using evaporated planar gold electrodes as described above. Appropriate set-ups for cone-and-plate rheological devices (Seebach et al. 2000; Fig. 13) and flow chambers (DePaola et al. 2001) have been developed. These set-ups have been used intensively to investigate the effect of laminar shear stress on the barrier function of various endothelia originating from diverse organs: BAEC (DePaola et al. 2001; Phelps and DePaola 2000), pulmonary trunk endothelial cells (PSECs; Seebach et al. 2000), HUVECs (Seebach et al. 2007) and human lymphatic endothelial cells (Breslin and Kurtz 2009). Surprisingly, all these different cell types show a similar reaction to a stepwise increase in shear stress, indicating that a common mechanism is responsible for the flow-dependent regulation of paracellular barrier function. Within the first few minutes, shear stress induces a dose-dependent and reversible increase in electrical resistance (Breslin and Kurtz 2009; DePaola et al. 2001; Seebach et al. 2000, 2007; Fig. 14a). This increase is associated with shear-stress-induced rac1 activation (Y. Liu et al. 2013; Seebach et al. 2007), a recruitment of actin, paxilin, GIT-2, rac1 and FAK to the junctions and a reorganization of VE-cadherin (Birukov et al. 2002; Seebach et al. 2007; Shikata et al. 2005). Inhibition of rac1 blocks both the increase in TER and the reorganization of F-actin and VE-cadherin (Breslin and Kurtz 2009; Seebach et al. 2007), indicating that rac1 is essential for the early shear-stress-induced strengthening of endothelial cell-cell junctions. For lymphatic endothelial cells, the inhibition of protein kinase A has been shown to have no effect on the early shear-stress-induced TER increase (Breslin and Kurtz 2009). In contrast to the cell types listed above, human glomerular endothelial cells exhibit a quick shear-stress-induced and NO-dependent decrease in TER (Bevan et al. 2011) indicating some organ-specific differences in the early response to laminar shear stress.

In contrast to microvascular endothelial cells that are derived from the blood brain barrier and that respond to prolonged shear stress by an increased expression of tight junction proteins and TER (Cucullo et al. 2011; Walsh et al. 2011), the TER of HUVECs (Seebach et al. 2007), PSECs (Seebach et al. 2000) and BAECs (DePaola et al. 2001; Phelps and DePaola 2000) is reduced within hours. This decrease is accompanied by the reorganization of junctional proteins, cell elongation and cell alignment in the direction of flow (Dieterich et al. 2000; Noria et al. 1999; Sakamoto et al. 2010; Seebach et al. 2000, 2007). After 24 h, the TER of HUVECs subjected to 12 dyn/cm^2 is reduced by 20-30 % and remains reduced for another 24 h if shear stress application is maintained (Seebach et al. 2007; Fig. 14b). Paradoxically, several immunohistological studies indicate that VE-cadherin-mediated cell-cell interactions were maintained or even enhanced after 24–48 h (Chien 2008; Noria et al. 1999; Sakamoto et al. 2010; Seebach et al. 2007), irrespective of a transient dissociation of some junctional proteins during the first few hours of the reorganization process (Noria et al. 1999; Sakamoto et al. 2010; Ukropec et al. 2002). A possible explanation for this discrepancy is that shear stress induces an increase in the linear amount of paracellular elements (lp) as discussed above. Indeed, a quantification of lp has shown an increase after 24 h of shear stress application by more than 50 %. This increase is mostly attributable to the elongation of the cells and, to a lesser extent, to a reduction of the cell size. This latter effect is probably the result of an anti-apoptotic effect of laminar shear stress. A normalization of measured TER values to lp has actually revealed that the shear-stress-induced TER decrease is caused by an increase of lp and not by a change of the specific junctional resistance (Seebach et al. 2007). These data indicate that shear-stress-induced

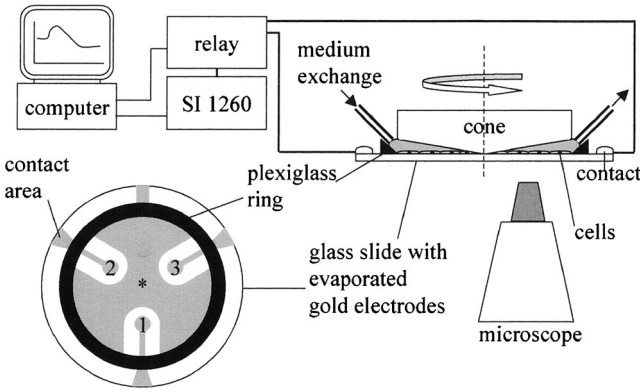

Fig. 13 Experimental set-up to determine TER under flow conditions. Representation of a cone and plate rheological in-vitro system to generate defined levels of shear stress over cultured cells. Metal electrodes evaporated onto the surface of a circular glass slide are connected to a computer-controlled impedance analyzer via a relay. Continuous medium exchange can be performed through capillaries. The cell layer can be examined by a phase-contrast microscope during shear stress application and images can be recorded automatically (*asterisk* counter electrode, *1–3* measuring electrodes). From Seebach et al. (2000)

transformation into an elongated and streamlined morphology is not only an adaptation to reduce hydrodynamic resistance

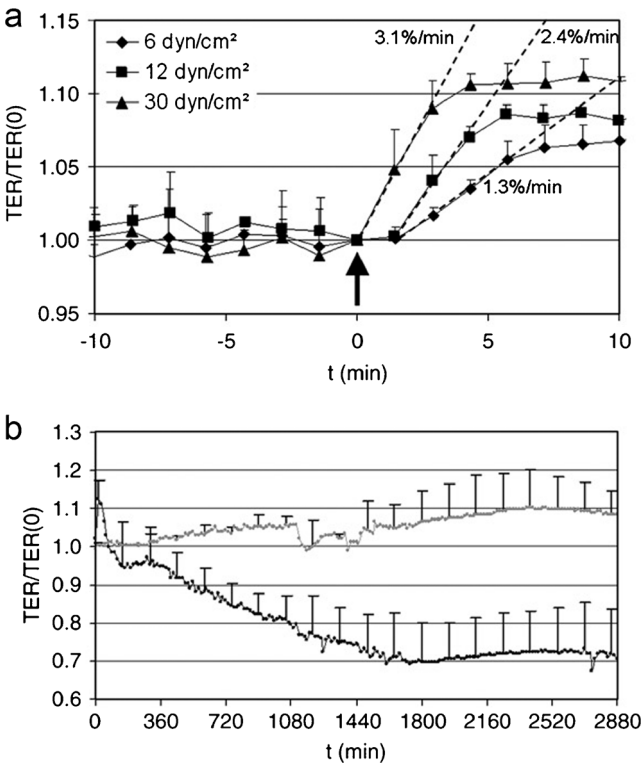

Fig. 14 Time course of TER under fluid shear stress. **a** Various shear stress levels were applied to a confluent human umbilical vein endothelial cell (HUVEC) monolayer. The TER shows a dose-dependent increase within the first few minutes after shear stress application. **b** Prolonged shear stress application of 12 dyn/cm^2 shows a moderate TER decrease of about 25 %; this reaches a steady state value after about 24 h (*black curve*). A control experiment with low shear stress (0.5 dyn/cm^2) shows no significant changes (*gray curve*). From Seebach et al. (2007)

(Barbee et al. 1995; Davies et al. 2003) but also has an impact on paracellular endothelial permeability.

A destruction of the glycocalix by heparinase (Brower et al. 2010; Yao et al. 2007) and the inhibition of p38-mitogen-activated protein kinase (Azuma et al. 2001; Kadohama et al. 2006) or rho-GTPases (Li et al. 1999; Wojciak-Stothard and Ridley 2003) are able to block the shear-stress-induced cell elongation, indicating that this morphological adaptation is a tightly regulated process. Prolonged exposure to disturbed flow profiles also leads to a reduction of TER (Phelps and DePaola 2000). However, in contrast to laminar shear stress, this TER is not associated with cell elongation but with the appearance of intercellular gaps (Chien 2008; Miao et al. 2005; Ting et al. 2012).

The effect of shear stress on hydraulic conductivity and permeability to solutes has been reviewed recently (Tarbell 2010) and will therefore only be briefly addressed here. Whereas the effect of shear stress on TER is similar for various types of endothelial cell, the effect on the hydraulic conductivity shows characteristic differences between BAECs and HUVECs. Enhanced shear stress over 3 h induces a more than four-fold increase in hydraulic conductivity of BAECs; this can be largely attenuated by the inhibition of endothelial NOS (Chang et al. 2000). In contrast, HUVECs show only a transient increase with a maximum during the first hour of enhanced shear stress exposure (Pang et al. 2005), indicating a cell-type-specific effect of shear stress on hydraulic conductivity.

Even though studies under static conditions indicate that the major fraction of water transport occurs along paracellular pathways (Cancel et al. 2007), a recent study has demonstrated that prolonged shear stress application over 24 h increases the expression of aquaporin-1 (Mun et al. 2013), a membrane protein that is involved in endothelial fluid transport (Verkman 2002; Verkman 2006). The functional relevance of the enhanced aquaporin expression for a shear-stress-induced increase in transcellular water transport has yet to be investigated.

The permeability of albumin, which is usually transported via transcytosis through the endothelial monolayer (Komarova and Malik 2010), is also regulated by shear stress. Acute shear stress reversibly increases the permeability of both BAEC and PAEC, even at relative moderate shear stress levels (Jo et al. 1991; Warboys et al. 2010). In contrast, prolonged shear stress over several days reduces albumin transport by a phosphatidyl-inositol-3-kinase-NO-cGMP-dependent mechanism (Warboys et al. 2010). However, whether these effects are attributable to changes in vesicular transport or are related to other permeability pathways remains to be investigated.

Cyclic stretch

Similar to the positive effects of laminar shear stress, moderate cyclic stretch has been proposed to have a beneficial effect on

endothelial barrier function (Fujiwara 2003). This hypothesis is supported by immunhistological and biochemical studies showing that prolonged application of moderate stretch (5 %) for 24 h induces an upregulation of the tight junction proteins zonula occludens-1 and occludin in combination with an increased junctional localization of these proteins (Collins et al. 2006). Furthermore, moderate stretch (5 %) but not excessive stretch (18 %) induces a protective effect against thrombin-induced gap formation (Birukova et al. 2006).

Although these data show that cyclic stretch leads to a reorganization of endothelial junctions, direct measurements of the barrier functions are rare. Birukova et al. (2003) preconditioned endothelial cells for 2 days to various stretch levels and replated them on gold electrodes to analyze the TER response to thrombin; they showed that preconditioning with moderate stretch (5 %) reduces the thrombin-induced loss of barrier function compared with unstretched control cells, whereas preconditioning with excessive stretch (18 %) enhances barrier breakdown. In a similar approach, preconditioning with moderate cyclic stretch (5 %) for 24 h has been demonstrated to reduce the permeability of endothelial cells to FITC-dextran (Collins et al. 2006), indicating that prolonged stretch application leads to changes in endothelial phenotype.

Recently, a new methodical approach has been developed to analyze the permeability of endothelial cells under stretch (Dubrovskyi et al. 2013) with high lateral resolution. This assay, which is described in detail above, allows direct evidence to be gained showing that the application of cyclic stretch of 18 % for 2 h leads to an increase of paracellular permeability.

Combination of various mechanical forces

The data summarized in this section clearly show that mechanical forces have a strong influence on the structure and function of endothelial cell-cell junctions. In-vivo-like mechanical loading presumably provides differentiation signals that are necessary for the expression of the barrier function that is specific for a given endothelial type. Notably, we need to recognize that adapted endothelial cells might react quite differently to external stimuli compared with endothelial cells that have been cultivated under normal conditions. Although progress has been made in understanding the individual effects of these

Table 3 Comparison summarizing the characteristics of the four techniques described in this review for the quantification of endothelial barrier function (+ yes, − no)

Character/requirement/ treatment	Permeability to inorganic ions; transendothelial electrical resistance		Permability to molecular probes	Permeability to water
	Direct current	Impedance spectroscopy		
Transport route	Mostly paracellular	Mostly paracellular	Probe-dependent	Mostly paracellular
Additional information from measurement	−	Capacitance of cell membranes, impedance of cell-substrate contact, temperature shift	−	−
Experimental equipment	Constant current source and voltmeter	Impedance analyzer	Fluorescence reader, spectrophotometer	Mostly self-developed set-ups[a]
Time resolution	Seconds to minutes	Seconds to minutes	Several minutes with manual sampling; real time set-ups possible	Depends on set-up; real time set-ups possible[a]
Growth substrates	Filter	Filter, conductive solid substrates	Filter, solid substrates[b]	Filter
Microscopic observation and barrier analysis at the same time	−	+	−	−
Cell-free reference needed	+	−	+	+
Multiwell formats available	+		+[b]	−
Similar methods with lateral resolution	Scanning ion conductance microscopy, voltage scanning		Scanning electrochemical microscopy, macroporous substrates, XPert assay[b]	−
Application of shear stress	+		+	+
Application of stretch	−		+	−
Application of hydrostatic pressure	+		+	+

[a] Sill et al. 1995

[b] Dubrovskyi et al. 2013

stimuli on endothelial barrier function, many open questions remain to be answered. A new challenge is to investigate the effect of combined forces. For example, as has recently been proposed, disturbed flow is not the only factor inducing atherosclerosis; the combination with circumferential stress might be a more potent initiator of plaque formation (Anssari-Benam and Korakianitis 2013). Indeed, the interplay between shear stress and cyclic stretch has been shown to be able to alter the expression of tight junction proteins and the rate of apoptosis (Berardi and Tarbell 2009). An appropriate experimental set-up to address this problem has been recently proposed (Huh et al. 2010).

Summary and outlook

In the last few decades, great efforts have been made to develop and improve the accuracy, time resolution and handling of various experimental set-ups for the investigation of endothelial barrier function. Table 3 provides a comparison of the existing approaches together with their individual specifications. The paragraph below briefly summarizes the current trends and developments in the field that might pave the way to a more detailed, sometimes unprecedented, functional analysis of barrier-forming cell junctions.

Technical advances enabled by micro- and nanotechnology

The large progress in micro- and nanotechnology in recent years has allowed the miniaturization of various set-ups and cell-based assays. On the one hand, this has led to the development of multi-well assays for TER and P_E measurements that provide the technical basis for at least medium sample throughput and, in some cases, even high throughput applications in drug development and drug targeting. On the other hand, miniaturization allows the analysis of endothelial barrier function at subcellular resolution in more fundamental cell biology. These approaches will provide more insight into junctional heterogeneity along individual cells or within cell ensembles and shed light on the regulation and fine-tuning of transcellular versus paracellular transport and permeation. In particular, little quantitative data describing the permeability of transcellular channels and fenestrae exist, even though these structures are of critical importance for understanding endothelial physiology in certain parts of the vasculature.

Combination with other techniques (multi-parametric analysis)

Approaches relying on cell growth upon conducting surfaces have been successfully combined with other independent readout techniques that are not necessarily sensitive for endothelial barrier function. The idea of these hybrid devices is to monitor endothelial cells from more than one perspective and to allow multi-parametric monitoring. For instance, ECIS monitoring of adherent cells has been combined with SPR, an optical biosensing principle that is widespread in biomolecular interaction analysis. SPR also requires cell growth on a thin gold-film and has proven to be highly sensitive to cytoskeletal rearrangements and cell volume changes (Robelek and Wegener 2010). SPR alone has been used intensively as a readout tool in cell-based GPCR and signal transduction research. In combination with ECIS (Michaelis et al. 2013), SPR might allow cytoskeletal and barrier changes to be detected simultaneously from the same cell population, thus extending the obtained information content considerably. Combining ECIS with other devices that report on cells grown on conducting surfaces is straightforward; such new combinations with other sensing principles might be electrochemical, piezoelectric, or optical in nature. Moreover, since metal electrodes are usually evaporated onto optically transparent substrates, they can also be combined with imaging devices, in particular, with light microscopic observation. The use of optically transparent electrode materials is a further step forward in the examination of function/structure relationships within one and the same cell monolayer (Choi et al. 2007).

Mechanical environment

The influence of mechanical forces on endothelial barrier function has been the focus of several studies in the last decade. These studies have suggested that various mechanical loads have a significant impact on endothelial differentiation in general and endothelial barrier function in particular. Thus, future developments of devices addressing endothelial biology will aim to enable the study of cells under fluid flow, so that experiments more closely mimic the in vivo situation. Microfluidics is probably the most versatile approach in this context, as it allows the application of well-defined shear stress to cells reared in channels; this method requires only small cell populations and provides the technical requirements for automated liquid handling.

References

Aird WC (2007a) Phenotypic heterogeneity of the endothelium. I. Structure, function, and mechanisms. Circ Res 100:158–173

Aird WC (2007b) Phenotypic heterogeneity of the endothelium. II. Representative vascular beds. Circ Res 100:174–190

Aird WC (2012) Endothelial cell heterogeneity. Cold Spring Harbor Perspect Med 2:a006429

Aman J, Bezu J van, Damanafshan A, Huveneers S, Eringa EC, Vogel SM, Groeneveld AB, Vonk Noordegraaf A, Hinsbergh VW van, Nieuw Amerongen GP van (2012) Effective treatment of edema and

endothelial barrier dysfunction with imatinib. Circulation 126: 2728–2738
Anssari-Benam A, Korakianitis T (2013) Atherosclerotic plaques: is endothelial shear stress the only factor? Med Hypotheses 81:235–239
Arndt S, Seebach J, Psathaki K, Galla HJ, Wegener J (2004) Bioelectrical impedance assay to monitor changes in cell shape during apoptosis. Biosens Bioelectron 19:583–594
Azuma N, Akasaka N, Kito H, Ikeda M, Gahtan V, Sasajima T, Sumpio BE (2001) Role of p38 MAP kinase in endothelial cell alignment induced by fluid shear stress. Am J Physiol Heart Circ Physiol 280: H189–H197
Barbee KA, Mundel T, Lal R, Davies PF (1995) Subcellular distribution of shear stress at the surface of flow-aligned and nonaligned endothelial monolayers. Am J Physiol 268:H1765–H1772
Barsoukov E, Macdonald JR (2005) Impedance spectroscopy. Wiley, New York
Bates DO (2010) Vascular endothelial growth factors and vascular permeability. Cardiovasc Res 87:262–271
Becker BF, Chappell D, Jacob M (2010) Endothelial glycocalyx and coronary vascular permeability: the fringe benefit. Basic Res Cardiol 105:687–701
Berardi DE, Tarbell JM (2009) Stretch and shear interactions affect intercellular junction protein expression and turnover in endothelial cells. Cel Mol Bioeng 2:320–331
Bergner S, Vatsyayan P, Matysik FM (2013) Recent advances in high resolution scanning electrochemical microscopy of living cells—a review. Anal Chim Acta 775:1–13
Betzen C, White R, Zehendner CM, Pietrowski E, Bender B, Luhmann HJ, Kuhlmann CR (2009) Oxidative stress upregulates the NMDA receptor on cerebrovascular endothelium. Free Radic Biol Med 47: 1212–1220
Bevan HS, Slater SC, Clarke H, Cahill PA, Mathieson PW, Welsh GI, Satchell SC (2011) Acute laminar shear stress reversibly increases human glomerular endothelial cell permeability via activation of endothelial nitric oxide synthase. Am J Physiol Renal Physiol 301: F733–F742
Birukov KG, Birukova AA, Dudek SM, Verin AD, Crow MT, Zhan X, DePaola N, Garcia JG (2002) Shear stress-mediated cytoskeletal remodeling and cortactin translocation in pulmonary endothelial cells. Am J Respir Cell Mol Biol 26:453–464
Birukov KG, Jacobson JR, Flores AA, Ye SQ, Birukova AA, Verin AD, Garcia JG (2003) Magnitude-dependent regulation of pulmonary endothelial cell barrier function by cyclic stretch. Am J Physiol Lung Cell Mol Physiol 285:L785–L797
Birukova AA, Chatchavalvanich S, Rios A, Kawkitinarong K, Garcia JG, Birukov KG (2006) Differential regulation of pulmonary endothelial monolayer integrity by varying degrees of cyclic stretch. Am J Pathol 168:1749–1761
Böcker M, Anczykowski B, Wegener JTS (2007) Scanning ion conductance microscopy with distance-modulated shear force control. Nanotechnology 18:145505
Bojarski C, Bendfeldt K, Gitter AH, Mankertz J, Fromm M, Wagner S, Riecken EO, Schulzke JD (2000) Apoptosis and intestinal barrier function. Ann N Y Acad Sci 915:270–274
Breslin JW, Kurtz KM (2009) Lymphatic endothelial cells adapt their barrier function in response to changes in shear stress. Lymphat Res Biol 7:229–237
Brower JB, Targovnik JH, Caplan MR, Massia SP (2010) High glucose-mediated loss of cell surface heparan sulfate proteoglycan impairs the endothelial shear stress response. Cytoskeleton 67:135–141
Buschmann MH, Dieterich P, Adams NA, Schnittler HJ (2005) Analysis of flow in a cone-and-plate apparatus with respect to spatial and temporal effects on endothelial cells. Biotechnol Bioeng 89:493–502
Cancel LM, Fitting A, Tarbell JM (2007) In vitro study of LDL transport under pressurized (convective) conditions. Am J Physiol Heart Circ Physiol 293:H126–H132
Carpi-Medina P, Whittembury G (1988) Comparison of transcellular and transepithelial water osmotic permeabilities (Pos) in the isolated proximal straight tubule (PST) of the rabbit kidney. Pflugers Arch 412:66–74
Chang YS, Yaccino JA, Lakshminarayanan S, Frangos JA, Tarbell JM (2000) Shear-induced increase in hydraulic conductivity in endothelial cells is mediated by a nitric oxide-dependent mechanism. Arterioscler Thromb Vasc Biol 20:35–42
Chen XL, Varner SE, Rao AS, Grey JY, Thomas S, Cook CK, Wasserman MA, Medford RM, Jaiswal AK, Kunsch C (2003) Laminar flow induction of antioxidant response element-mediated genes in endothelial cells. A novel anti-inflammatory mechanism. J Biol Chem 278:703–711
Chien S (2008) Effects of disturbed flow on endothelial cells. Ann Biomed Eng 36:554–562
Choi CK, English AE, Jun SI, Kihm KD, Rack PD (2007) An endothelial cell compatible biosensor fabricated using optically thin indium tin oxide silicon nitride electrodes. Biosens Bioelectron 22:2585–2590
Claude P (1978) Morphological factors influencing transepithelial permeability: a model for the resistance of the zonula occludens. J Membr Biol 39:219–232
Cohen AW, Carbajal JM, Schaeffer RC (1999) VEGF stimulates tyrosine phosphorylation of beta-catenin and small-pore endothelial barrier dysfunction. Am J Physiol Heart Circ Physiol 277:H2038–H2049
Collins NT, Cummins PM, Colgan OC, Ferguson G, Birney YA, Murphy RP, Meade G, Cahill PA (2006) Cyclic strain-mediated regulation of vascular endothelial occludin and ZO-1: influence on intercellular tight junction assembly and function. Arterioscler Thromb Vasc Biol 26:62–68
Conway DE, Breckenridge MT, Hinde E, Gratton E, Chen CS, Schwartz MA (2013) Fluid shear stress on endothelial cells modulates mechanical tension across VE-cadherin and PECAM-1. Curr Biol 23: 1024–1030
Cucullo L, Hossain M, Puvenna V, Marchi N, Janigro D (2011) The role of shear stress in blood–brain barrier endothelial physiology. BMC Neurosci 12:40
Curtis TM, Tabb J, Romeo L, Schwager SJ, Widder MW, Schalie WH van der (2009a) Improved cell sensitivity and longevity in a rapid impedance-based toxicity sensor. J Appl Toxicol 29:374–380
Curtis TM, Widder MW, Brennan LM, Schwager SJ, Schalie WH van der, Fey J, Salazar N (2009b) A portable cell-based impedance sensor for toxicity testing of drinking water. Lab Chip 9:2176–2183
Dartsch PC, Betz E (1989) Response of cultured endothelial cells to mechanical stimulation. Basic Res Cardiol 84:268–281
Davies PF (1991) Mechanical sensing mechanisms: shear stress and endothelial cells. J Vasc Surg 13:729–731
Davies PF (1997) Overview: temporal and spatial relationships in shear stress-mediated endothelial signalling. J Vasc Res 34:208–211
Davies PF, Dewey CF Jr, Bussolari SR, Gordon EJ, Gimbrone MA Jr (1984) Influence of hemodynamic forces on vascular endothelial function. In vitro studies of shear stress and pinocytosis in bovine aortic cells. J Clin Invest 73:1121–1129
Davies PF, Remuzzi A, Gordon EJ, Dewey CF Jr, Gimbrone MA Jr (1986) Turbulent fluid shear stress induces vascular endothelial cell turnover in vitro. Proc Natl Acad Sci U S A 83:2114–2117
Davies PF, Zilberberg J, Helmke BP (2003) Spatial microstimuli in endothelial mechanosignaling. Circ Res 92:359–370
Deen WM, Lazzara MJ, Myers BD (2001) Structural determinants of glomerular permeability. Am J Physiol Renal Physiol 281:F579–F596
Dejana E, Orsenigo F (2013) Endothelial adherens junctions at a glance. J Cell Sci 126:2545–2549

DeMaio L, Tarbell JM, Scaduto RC Jr, Gardner TW, Antonetti DA (2004) A transmural pressure gradient induces mechanical and biological adaptive responses in endothelial cells. Am J Physiol Heart Circ Physiol 286:H731–H741

DePaola N, Phelps JE, Florez L, Keese CR, Minnear FL, Giaever I, Vincent P (2001) Electrical impedance of cultured endothelium under fluid flow. Ann Biomed Eng 29:648–656

Dewey CF Jr, Bussolari SR, Gimbrone MA Jr, Davies PF (1981) The dynamic response of vascular endothelial cells to fluid shear stress. J Biomech Eng 103:177–185

Dieterich P, Odenthal-Schnittler M, Mrowietz C, Kramer M, Sasse L, Oberleithner H, Schnittler HJ (2000) Quantitative morphodynamics of endothelial cells within confluent cultures in response to fluid shear stress. Biophys J 79:1285–1297

Dimmeler S, Haendeler J, Rippmann V, Nehls M, Zeiher AM (1996) Shear stress inhibits apoptosis of human endothelial cells. FEBS Lett 399:71–74

Dubrovskyi O, Birukova AA, Birukov KG (2013) Measurement of local permeability at subcellular level in cell models of agonist- and ventilator-induced lung injury. Lab Invest 93:254–263

Dvorak AM, Feng D (2001) The vesiculo-vacuolar organelle (VVO). A new endothelial cell permeability organelle. J Histochem Cytochem 49:419–432

Emmanuel C, Huynh M, Matthews J, Kelly E, Zoellner H (2013) TNF-alpha and TGF-beta synergistically stimulate elongation of human endothelial cells without transdifferentiation to smooth muscle cell phenotype. Cytokine 61:38–40

Erben M, Decker S, Franke H, Galla HJ (1995) Electrical resistance measurements on cerebral capillary endothelial cells—a new technique to study small surface areas. J Biochem Biophys Methods 30:227–238

Esser S, Wolburg K, Wolburg H, Breier G, Kurzchalia T, Risau W (1998) Vascular endothelial growth factor induces endothelial fenestrations in vitro. J Cell Biol 140:947–959

Fischbarg J, Lim JJ (1973) Determination of the impedance locus of rabbit corneal endothelium. Biophys J 13:595–599

FitzGerald OM, Hess EV, Chance A, Highsmith RF (1987) Quantitative studies of human monokine-induced endothelial cell elongation. J Leukoc Biol 41:421–428

Fordjour AK, Harrington EO (2009) PKCdelta influences p190 phosphorylation and activity: events independent of PKCdelta-mediated regulation of endothelial cell stress fiber and focal adhesion formation and barrier function. Biochim Biophys Acta 1790:1179–1190

Franke RP, Grafe M, Schnittler H, Seiffge D, Mittermayer C, Drenckhahn D (1984) Induction of human vascular endothelial stress fibres by fluid shear stress. Nature 307:648–649

Freiesleben-de Blasio B, Wegener J (2006) Impedance spectroscopy. Encyclopedia of medical technologies and instrumentation. Wiley, Chichester

Fu BM, Tarbell JM (2013) Mechano-sensing and transduction by endothelial surface glycocalyx: composition, structure, and function. Wiley Interdisc Rev Syst Biol Med 5:381–390

Fujiwara K (2003) Mechanical stresses keep endothelial cells healthy: beneficial effects of a physiological level of cyclic stretch on endothelial barrier function. Am J Physiol Lung Cell Mol Physiol 285: L782–L784

Giaever I, Keese CR (1984) Monitoring fibroblast behavior in tissue culture with an applied electric field. Proc Natl Acad Sci U S A 81:3761–3764

Giaever I, Keese CR (1991) Micromotion of mammalian cells measured electrically. Proc Natl Acad Sci U S A 88:7896–7900

Gitter AH, Bertog M, Schulzke J, Fromm M (1997) Measurement of paracellular epithelial conductivity by conductance scanning. Pflugers Arch 434:830–840

Gitter AH, Wullstein F, Fromm M, Schulzke JD (2001) Epithelial barrier defects in ulcerative colitis: characterization and quantification by electrophysiological imaging. Gastroenterology 121:1320–1328

Gorelik J, Gu Y, Spohr HA, Shevchuk AI, Lab MJ, Harding SE, Edwards CR, Whitaker M, Moss GW, Benton DC, Sanchez D, Darszon A, Vodyanoy I, Klenerman D, Korchev YE (2002) Ion channels in small cells and subcellular structures can be studied with a smart patch-clamp system. Biophys J 83:3296–3303

Gorelik J, Zhang Y, Shevchuk AI, Frolenkov GI, Sanchez D, Lab MJ, Vodyanoy I, Edwards CR, Klenerman D, Korchev YE (2004) The use of scanning ion conductance microscopy to image A6 cells. Mol Cell Endocrinol 217:101–108

Grab DJ, Nyarko E, Nikolskaia OV, Kim YV, Dumler JS (2009) Human brain microvascular endothelial cell traversal by *Borrelia burgdorferi* requires calcium signaling. Clin Microbiol Infect 15: 422–426

Grabowski EF, Jaffe EA, Weksler BB (1985) Prostacyclin production by cultured endothelial cell monolayers exposed to step increases in shear stress. J Lab Clin Med 105:36–43

Grimnes S, Martinsen OG (2000) Bioimpedance and bioelectricity basics. Academic Press, Cornwall

Gunzel D, Krug SM, Rosenthal R, Fromm M (2010) Biophysical methods to study tight junction permeability. Curr Top Membr 65:39–78

Gunzel D, Zakrzewski SS, Schmid T, Pangalos M, Wiedenhoeft J, Blasse C, Ozboda C, Krug SM (2012) From TER to trans- and paracellular resistance: lessons from impedance spectroscopy. Ann N Y Acad Sci 1257:142–151

Hartmann C, Zozulya A, Wegener J, Galla HJ (2007) The impact of glia-derived extracellular matrices on the barrier function of cerebral endothelial cells: an in vitro study. Exp Cell Res 313:1318–1325

Heffernan M, Chance A, Hess EV, Highsmith RF, FitzGerald O (1994) Alterations in human endothelial cell morphology, proliferation and function by a macrophage-derived factor. Irish J Med Sci 163:359–365

Hierck BP, Van der Heiden K, Alkemade FE, Van de Pas S, Van Thienen JV, Groenendijk BC, Bax WH, Van der Laarse A, Deruiter MC, Horrevoets AJ, Poelmann RE (2008) Primary cilia sensitize endothelial cells for fluid shear stress. Dev Dyn 237:725–735

Hordijk PL, Anthony E, Mul FP, Rientsma R, Oomen LC, Roos D (1999) Vascular-endothelial-cadherin modulates endothelial monolayer permeability. J Cell Sci 112:1915–1923

Hu G, Place AT, Minshall RD (2008) Regulation of endothelial permeability by Src kinase signaling: vascular leakage versus transcellular transport of drugs and macromolecules. Chem Biol Interact 171: 177–189

Huh D, Matthews BD, Mammoto A, Montoya-Zavala M, Hsin HY, Ingber DE (2010) Reconstituting organ-level lung functions on a chip. Science 328:1662–1668

Ishida T, Takahashi M, Corson MA, Berk BC (1997) Fluid shear stress-mediated signal transduction: how do endothelial cells transduce mechanical force into biological responses? Ann N Y Acad Sci 811: 12–23

Jacob M, Chappell D (2013) Reappraising Starling: the physiology of the microcirculation. Curr Opin Crit Care 19:282–289

Janshoff A, Wegener J, Sieber M, Galla HJ (1996) Double-mode impedance analysis of epithelial cell monolayers cultured on shear wave resonators. Eur Biophys J 25:93–103

Jo H, Dull RO, Hollis TM, Tarbell JM (1991) Endothelial albumin permeability is shear dependent, time dependent, and reversible. Am J Physiol 260:H1992–H1996

Jovov B, Wills NK, Lewis SA (1991) A spectroscopic method for assessing confluence of epithelial cell cultures. Am J Physiol 261: C1196–C1203

Kadohama T, Akasaka N, Nishimura K, Hoshino Y, Sasajima T, Sumpio BE (2006) p38 Mitogen-activated protein kinase activation in endothelial cell is implicated in cell alignment and elongation induced by fluid shear stress. Endothelium 13:43–50

Kataoka N, Iwaki K, Hashimoto K, Mochizuki S, Ogasawara Y, Sato M, Tsujioka K, Kajiya F (2002) Measurements of endothelial cell-to-

cell and cell-to-substrate gaps and micromechanical properties of endothelial cells during monocyte adhesion. Proc Natl Acad Sci U S A 99:15638–15643

Keese CR, Bhawe K, Wegener J, Giaever I (2002) Real-time impedance assay to follow the invasive activities of metastatic cells in culture. Biotechniques 33:842–850

Keese CR, Wegener J, Walker SR, Giaever I (2004) Electrical wound-healing assay for cells in vitro. Proc Natl Acad Sci U S A 101:1554–1559

Keil JM, Liu X, Antonetti DA (2013) Glucocorticoid induction of occludin expression and endothelial barrier requires transcription factor p54 NONO. Invest Ophthalmol Vis Sci 54:4007–4015

Komarova Y, Malik AB (2010) Regulation of endothelial permeability via paracellular and transcellular transport pathways. Annu Rev Physiol 72:463–493

Koslow AR, Stromberg RR, Friedman LI, Lutz RJ, Hilbert SL, Schuster P (1986) A flow system for the study of shear forces upon cultured endothelial cells. J Biomech Eng 108:338–341

Kottra G, Fromter E (1984a) Rapid determination of intraepithelial resistance barriers by alternating current spectroscopy. I. Experimental procedures. Pflugers Arch 402:409–420

Kottra G, Fromter E (1984b) Rapid determination of intraepithelial resistance barriers by alternating current spectroscopy. II. Test of model circuits and quantification of results. Pflugers Arch 402:421–432

Krug SM, Fromm M, Gunzel D (2009) Two-path impedance spectroscopy for measuring paracellular and transcellular epithelial resistance. Biophys J 97:2202-2211

Lamontagne D, Pohl U, Busse R (1992) Mechanical deformation of vessel wall and shear stress determine the basal release of endothelium-derived relaxing factor in the intact rabbit coronary vascular bed. Circ Res 70:123–130

Levesque MJ, Nerem RM (1985) The elongation and orientation of cultured endothelial cells in response to shear stress. J Biomech Eng 107:341–347

Li S, Chen BP, Azuma N, Hu YL, Wu SZ, Sumpio BE, Shyy JY, Chien S (1999) Distinct roles for the small GTPases Cdc42 and Rho in endothelial responses to shear stress. J Clin Invest 103:1141–1150

Lim JJ, Fischbarg J (1981) Electrical properties of rabbit corneal endothelium as determined from impedance measurements. Biophys J 36:677–695

Liu CL, Tam JC, Sanders AJ, Ko CH, Fung KP, Leung PC, Harding KG, Jiang WG, Lau CB (2013) Molecular angiogenic events of a two-herb wound healing formula involving MAPK and Akt signaling pathways in human vascular endothelial cells. Wound Repair Regen 21:579–587

Liu Y, Collins C, Kiosses WB, Murray AM, Joshi M, Shepherd TR, Fuentes EJ, Tzima E (2013) A novel pathway spatiotemporally activates Rac1 and redox signaling in response to fluid shear stress. J cell Biol 201:863–873

Lo CM, Keese CR, Giaever I (1994) pH changes in pulsed CO_2 incubators cause periodic changes in cell morphology. Exp Cell Res 213:391–397

Lo CM, Keese CR, Giaever I (1999) Cell-substrate contact: another factor may influence transepithelial electrical resistance of cell layers cultured on permeable filters. Exp Cell Res 250:576–580

Lohmann C, Huwel S, Galla HJ (2002) Predicting blood–brain barrier permeability of drugs: evaluation of different in vitro assays. J Drug Target 10:263–276

Lvovich VF (2012) Impedance spectroscopy: applications to electrochemical and dielectric phenomena. Wiley, New York

Mahringer A, Ott M, Reimold I, Reichel V, Fricker G (2011) The ABC of the blood–brain barrier—regulation of drug efflux pumps. Curr Pharm Des 17:2762–2770

Matter K, Balda MS (2003) Functional analysis of tight junctions. Methods 30:228–234

McKenzie JA, Ridley AJ (2007) Roles of Rho/ROCK and MLCK in TNF-alpha-induced changes in endothelial morphology and permeability. J Cell Physiol 213:221–228

Miao H, Hu YL, Shiu YT, Yuan S, Zhao Y, Kaunas R, Wang Y, Jin G, Usami S, Chien S (2005) Effects of flow patterns on the localization and expression of VE-cadherin at vascular endothelial cell junctions: in vivo and in vitro investigations. J Vasc Res 42:77–89

Michaelis S, Rommel CE, Endell J, Goring P, Wehrspohn R, Steinem C, Janshoff A, Galla HJ, Wegener J (2012) Macroporous silicon chips for laterally resolved, multi-parametric analysis of epithelial barrier function. Lab Chip 12:2329–2336

Michaelis S, Wegener J, Robelek R (2013) Label-free monitoring of cell-based assays: combining impedance analysis with SPR for multiparametric cell profiling. Biosens Bioelectron 49:63–70

Miller DS, Cannon RE (2013) Signaling pathways that regulate basal ABC transporter activity at the blood–brain barrier. Curr Pharm Des (in press)

Moy AB, Winter M, Kamath A, Blackwell K, Reyes G, Giaever I, Keese C, Shasby DM (2000) Histamine alters endothelial barrier function at cell-cell and cell-matrix sites. Am J Physiol Lung Cell Mol Physiol 278:L888–L898

Mun GI, Jang SI, Boo YC (2013) Laminar shear stress induces the expression of aquaporin 1 in endothelial cells involved in wound healing. Biochem Biophys Res Commun 430:554–559

Naruse K, Yamada T, Sokabe M (1998) Involvement of SA channels in orienting response of cultured endothelial cells to cyclic stretch. Am J Physiol 274:H1532–H1538

Nauli SM, Kawanabe Y, Kaminski JJ, Pearce WJ, Ingber DE, Zhou J (2008) Endothelial cilia are fluid shear sensors that regulate calcium signaling and nitric oxide production through polycystin-1. Circulation 117:1161–1171

Neuhaus W, Bogner E, Wirth M, Trzeciak J, Lachmann B, Gabor F, Noe CR (2006) A novel tool to characterize paracellular transport: the APTS-dextran ladder. Pharm Res 23:1491–1501

Noria S, Cowan DB, Gotlieb AI, Langille BL (1999) Transient and steady-state effects of shear stress on endothelial cell adherens junctions. Circ Res 85:504–514

Novak P, Li C, Shevchuk AI, Stepanyan R, Caldwell M, Hughes S, Smart TG, Gorelik J, Ostanin VP, Lab MJ, Moss GW, Frolenkov GI, Klenerman D, Korchev YE (2009) Nanoscale live-cell imaging using hopping probe ion conductance microscopy. Nat Methods 6:279–281

Opp D, Wafula B, Lim J, Huang E, Lo JC, Lo CM (2009) Use of electric cell-substrate impedance sensing to assess in vitro cytotoxicity. Biosens Bioelectron 24:2625–2629

Orazem ME, Tribollet B (2008) Electrochemical impedance spectroscopy. Wiley, New York

Pajkossy T (1994) Impedance of rough capacitive electrodes. J Electroanal Chem 364:111–125

Pang Z, Antonetti DA, Tarbell JM (2005) Shear stress regulates HUVEC hydraulic conductivity by occludin phosphorylation. Ann Biomed Eng 33:1536–1545

Parker JC, Stevens T, Randall J, Weber DS, King JA (2006) Hydraulic conductance of pulmonary microvascular and macrovascular endothelial cell monolayers. Am J Physiol Lung Cell Mol Physiol 291:L30–L37

Patterson CE, Lum H (2001) Update on pulmonary edema: the role and regulation of endothelial barrier function. Endothelium 8:75–105

Phelps JE, DePaola N (2000) Spatial variations in endothelial barrier function in disturbed flows in vitro. Am J Physiol Heart Circ Physiol 278:H469–H476

Poelmann RE, Van der Heiden K, Gittenberger-de Groot A, Hierck BP (2008) Deciphering the endothelial shear stress sensor. Circulation 117:1124–1126

Powell DW (1981) Barrier function of epithelia. Am J Physiol 241:G275–G288

Predescu SA, Predescu DN, Malik AB (2007) Molecular determinants of endothelial transcytosis and their role in endothelial permeability. Am J Physiol Lung Cell Mol Physiol 293:L823–L842

Riha GM, Lin PH, Lumsden AB, Yao Q, Chen C (2005) Roles of hemodynamic forces in vascular cell differentiation. Ann Biomed Eng 33:772–779

Robelek R, Wegener J (2010) Label-free and time-resolved measurements of cell volume changes by surface plasmon resonance (SPR) spectroscopy. Biosens Bioelectron 25:1221–1224

Rothermel A, Nieber M, Muller J, Wolf P, Schmidt M, Robitzki AA (2006) Real-time measurement of PMA-induced cellular alterations by microelectrode array-based impedance spectroscopy. Biotechniques 41: 445–450

Sakamoto N, Segawa K, Kanzaki M, Ohashi T, Sato M (2010) Role of p120-catenin in the morphological changes of endothelial cells exposed to fluid shear stress. Biochem Biophys Res Commun 398: 426–432

Salmon AH, Neal CR, Harper SJ (2009) New aspects of glomerular filtration barrier structure and function: five layers (at least) not three. Curr Opin Nephrol Hypertens 18:197–205

Schnittler HJ (1998) Structural and functional aspects of intercellular junctions in vascular endothelium. Basic Res Cardiol 93 (Suppl 3): 30–39

Schnittler HJ, Franke RP, Akbay U, Mrowietz C, Drenckhahn D (1993) Improved in vitro rheological system for studying the effect of fluid shear stress on cultured cells. Am J Physiol 265:C289–C298

Schulzke JD, Bojarski C, Zeissig S, Heller F, Gitter AH, Fromm M (2006) Disrupted barrier function through epithelial cell apoptosis. Ann N Y Acad Sci 1072:288–299

Scott CW, Peters MF (2010) Label-free whole-cell assays: expanding the scope of GPCR screening. Drug Discov Today 15:704–716

Seebach J, Dieterich P, Luo F, Schillers H, Vestweber D, Oberleithner H, Galla HJ, Schnittler HJ (2000) Endothelial barrier function under laminar fluid shear stress. Lab Invest 80:1819–1831

Seebach J, Donnert G, Kronstein R, Werth S, Wojciak-Stothard B, Falzarano D, Mrowietz C, Hell SW, Schnittler HJ (2007) Regulation of endothelial barrier function during flow-induced conversion to an arterial phenotype. Cardiovasc Res 75:596–607

Shikata Y, Rios A, Kawkitinarong K, DePaola N, Garcia JG, Birukov KG (2005) Differential effects of shear stress and cyclic stretch on focal adhesion remodeling, site-specific FAK phosphorylation, and small GTPases in human lung endothelial cells. Exp Cell Res 304:40–49

Sill H, Butler C, Hollis T, Tarbell J (1992) Albumin permeability and electrical resistance as means of assessing endothelial monolayer integrity in vitro. J Tissue Cult Methods 14:253–257

Sill HW, Chang YS, Artman JR, Frangos JA, Hollis TM, Tarbell JM (1995) Shear stress increases hydraulic conductivity of cultured endothelial monolayers. Am J Physiol 268:H535–H543

Simard JM, Kent TA, Chen M, Tarasov KV, Gerzanich V (2007) Brain oedema in focal ischaemia: molecular pathophysiology and theoretical implications. Lancet Neurol 6:258–268

Simionescu M, Simionescu N, Palade GE (1975) Segmental differentiations of cell junctions in the vascular endothelium. The microvasculature. J Cell Biol 67:863–885

Simionescu M, Simionescu N, Palade GE (1976) Segmental differentiations of cell junctions in the vascular endothelium. Arteries and veins. J Cell Biol 68:705–723

Steinem C, Janshoff A, Wegener J, Ulrich WP, Willenbrink W, Sieber M, Galla HJ (1997) Impedance and shear wave resonance analysis of ligand-receptor interactions at functionalized surfaces and of cell monolayers. Biosens Bioelectron 12:787–808

Stolpen AH, Guinan EC, Fiers W, Pober JS (1986) Recombinant tumor necrosis factor and immune interferon act singly and in combination to reorganize human vascular endothelial cell monolayers. Am J Pathol 123:16–24

Stolwijk JA, Hartmann C, Balani P, Albermann S, Keese CR, Giaever I, Wegener J (2011) Impedance analysis of adherent cells after in situ electroporation: non-invasive monitoring during intracellular manipulations. Biosens Bioelectron 26:4720–4727

Sun C, Wu MH, Yuan SY (2011) Nonmuscle myosin light-chain kinase deficiency attenuates atherosclerosis in apolipoprotein E-deficient mice via reduced endothelial barrier dysfunction and monocyte migration. Circulation 124:48–57

Sun C, Wu MH, Lee ES, Yuan SY (2012) A disintegrin and metalloproteinase 15 contributes to atherosclerosis by mediating endothelial barrier dysfunction via Src family kinase activity. Arterioscler Thromb Vasc Biol 32:2444–2451

Suttorp N, Hessz T, Seeger W, Wilke A, Koob R, Lutz F, Drenckhahn D (1988) Bacterial exotoxins and endothelial permeability for water and albumin in vitro. Am J Physiol 255:C368–C376

Suttorp N, Fuchs T, Seeger W, Wilke A, Drenckhahn D (1989) Role of Ca^{2+} and Mg^{2+} for endothelial permeability of water and albumin in vitro. Lab Invest 61:183–191

Takahashi M, Ishida T, Traub O, Corson MA, Berk BC (1997) Mechanotransduction in endothelial cells: temporal signaling events in response to shear stress. J Vasc Res 34:212–219

Tarbell JM (2010) Shear stress and the endothelial transport barrier. Cardiovasc Res 87:320–330

Tarbell JM, Shi ZD (2013) Effect of the glycocalyx layer on transmission of interstitial flow shear stress to embedded cells. Biomech Model Mechanobiol 12:111–121

Tarbell JM, Demaio L, Zaw MM (1999) Effect of pressure on hydraulic conductivity of endothelial monolayers: role of endothelial cleft shear stress. J Appl Physiol 87:261–268

Taylor SL, Wahl-Jensen V, Copeland AM, Jahrling PB, Schmaljohn CS (2013) Endothelial cell permeability during hantavirus infection involves factor XII-dependent increased activation of the kallikrein-kinin system. PLoS Pathogens 9:e1003470

Terada LS (2008) What underlies endothelial shear sensing? The matrix, of course. Circ Res 103:562–564

Ting LH, Jahn JR, Jung JI, Shuman BR, Feghhi S, Han SJ, Rodriguez ML, Sniadecki NJ (2012) Flow mechanotransduction regulates traction forces, intercellular forces, and adherens junctions. Am J Physiol Heart Circ Physiol 302:H2220–H2229

Traub O, Berk BC (1998) Laminar shear stress: mechanisms by which endothelial cells transduce an atheroprotective force. Arterioscler Thromb Vasc Biol 18:677–685

Tsukahara H, Noiri E, Jiang MZ, Hiraoka M, Mayumi M (2000) Role of nitric oxide in human pulmonary microvascular endothelial cell adhesion. Life Sci 67:1–11

Turner MR (1992) Flows of liquid and electrical current through monolayers of cultured bovine arterial endothelium. J Physiol (Lond) 449: 1–20

Ukropec JA, Hollinger MK, Woolkalis MJ (2002) Regulation of VE-cadherin linkage to the cytoskeleton in endothelial cells exposed to fluid shear stress. Exp Cell Res 273:240–247

Vandoorne K, Addadi Y, Neeman M (2010) Visualizing vascular permeability and lymphatic drainage using labeled serum albumin. Angiogenesis 13:75–85

Verkman AS (2002) Aquaporin water channels and endothelial cell function. J Anat 200:617–627

Verkman AS (2006) Aquaporins in endothelia. Kidney Int 69:1120–1123

Vestweber D (2008) VE-cadherin: the major endothelial adhesion molecule controlling cellular junctions and blood vessel formation. Arterioscler Thromb Vasc Biol 28:223–232

Wallez Y, Huber P (2008) Endothelial adherens and tight junctions in vascular homeostasis, inflammation and angiogenesis. Biochim Biophys Acta 1778:794–809

Walsh TG, Murphy RP, Fitzpatrick P, Rochfort KD, Guinan AF, Murphy A, Cummins PM (2011) Stabilization of brain microvascular endothelial barrier function by shear stress involves VE-cadherin

signaling leading to modulation of pTyr-occludin levels. J Cell Physiol 226:3053–3063

Warboys CM, Eric Berson R, Mann GE, Pearson JD, Weinberg PD (2010) Acute and chronic exposure to shear stress have opposite effects on endothelial permeability to macromolecules. Am J Physiol Heart Circ Physiol 298:H1850–H1856

Wedel-Parlow M von, Schrot S, Lemmen J, Treeratanapiboon L, Wegener J, Galla HJ (2011) Neutrophils cross the BBB primarily on transcellular pathways: an in vitro study. Brain Res 1367:62–76

Wegener J, Sieber M, Galla HJ (1996) Impedance analysis of epithelial and endothelial cell monolayers cultured on gold surfaces. J Biochem Biophys Methods 32:151–170

Wegener J, Zink S, Rosen P, Galla H (1999) Use of electrochemical impedance measurements to monitor beta-adrenergic stimulation of bovine aortic endothelial cells. Pflugers Arch 437:925–934

Wegener J, Hakvoort A, Galla HJ (2000a) Barrier function of porcine choroid plexus epithelial cells is modulated by cAMP-dependent pathways in vitro. Brain Res 853:115–124

Wegener J, Keese CR, Giaever I (2000b) Electric cell-substrate impedance sensing (ECIS) as a noninvasive means to monitor the kinetics of cell spreading to artificial surfaces. Exp Cell Res 259:158–166

Wegener J, Abrams D, Willenbrink W, Galla HJ, Janshoff A (2004) Automated multi-well device to measure transepithelial electrical resistances under physiological conditions. Biotechniques 37:590–597

Wit C de (2010) Different pathways with distinct properties conduct dilations in the microcirculation in vivo. Cardiovasc Res 85:604–613

Wojciak-Stothard B, Ridley AJ (2003) Shear stress-induced endothelial cell polarization is mediated by Rho and Rac but not Cdc42 or PI 3-kinases. J Cell Biol 161:429–439

Xu Q (2009) Disturbed flow-enhanced endothelial turnover in atherosclerosis. Trends Cardiovasc Med 19:191–195

Yao Y, Rabodzey A, Dewey CF Jr (2007) Glycocalyx modulates the motility and proliferative response of vascular endothelium to fluid shear stress. Am J Physiol Heart Circ Physiol 293:H1023–H1030

Yin F, Watsky MA (2005) LPA and S1P increase corneal epithelial and endothelial cell transcellular resistance. Invest Ophthalmol Vis Sci 46:1927–1933

Yoshida Y, Okano M, Wang S, Kobayashi M, Kawasumi M, Hagiwara H, Mitsumata M (1995) Hemodynamic-force-induced difference of interendothelial junctional complexes. Ann N Y Acad Sci 748: 104–120

Young EF, Smilenov LB (2011) Impedance-based surveillance of transient permeability changes in coronary endothelial monolayers after exposure to ionizing radiation. Radiat Res 176:415–424

Young EW, Watson MW, Srigunapalan S, Wheeler AR, Simmons CA (2010) Technique for real-time measurements of endothelial permeability in a microfluidic membrane chip using laser-induced fluorescence detection. Anal Chem 82:808–816

Zink S, Rosen P, Sackmann B, Lemoine H (1993) Regulation of endothelial permeability by beta-adrenoceptor agonists: contribution of beta 1- and beta 2-adrenoceptors. Biochim Biophys Acta 1178:286–298